



Open Archive TOULOUSE Archive Ouverte (OATAO)

OATAO is an open access repository that collects the work of Toulouse researchers and makes it freely available over the web where possible.

This is an author-deposited version published in: <http://oatao.univ-toulouse.fr/>
Eprints ID: 17660

To cite this version: Paroissien, Eric and Gaubert, Frédéric and Da Veiga, Anthony and Lachaud, Frédéric *Elasto-Plastic Analysis of Bonded Joints with Macro-Elements*. (2013) Journal of Adhesion Science and Technology, vol. 27 (n° 13). pp. 1464-1498. ISSN 0169-4243

Official URL: <http://dx.doi.org/10.1080/01694243.2012.745053>

Any correspondence concerning this service should be sent to the repository administrator: staff-oatao@listes-diff.inp-toulouse.fr

Elasto-Plastic Analysis of Bonded Joints with Macro-Elements

E. PAROISSIEN^{1,*}, F. GAUBERT¹, A. DA VEIGA¹, F. LACHAUD²

¹*SOGETI HIGH TECH, Parc le Millénaire - Bât A1, Avenue de l'Escadrille Normandie
Niemen, 31700 BLAGNAC, FRANCE*

²*Institut Clément Ader, ISAE/DMSM, Campus ENSICA, 1 Place Emile Blouin, 31500
TOULOUSE*

Running Head: Elasto-Plastic Analysis of Bonded Joints

*To whom correspondence should be addressed: Tel. +33534362684, Fax.
+33534362626, E-mail: eric.paroissien@sogeti.com

Abstract – The Finite Element (FE) method could be able to address the stress analysis of bonded joints. Nevertheless, analyses based on FE models are mainly computationally cost expensive and it would be profitable to develop simplified approaches, enabling extensive parametric studies. Firstly, a 1D-bar and 1D-beam simplified models for the bonded joint stress analysis, assuming a linear elastic adhesive material, are presented. These models derive from an approach, inspired by the finite element (FE) method using a formulation based on a 4-node macro-element, which is able to simulate an entire bonded overlap. Moreover, a linear shear stress variation in the adherend thickness is included in the formulation. Secondly, a numerical procedure is then presented to introduce into both models an elasto-plastic adhesive material behavior, while keeping the previous linear elastic formulation. Finally, assuming an elastic perfectly plastic adhesive material behavior, the results produced by simplified models are compared with the results predicted by FE using 1D-bar, plane stress and 3D models. Good agreements are shown.

keywords: *bonded joint, single-lap shear, non-linear material adhesive, Finite Element method, analytical formulation, macro-element*

NOMENCLATURE AND UNITS

A_j	extensional stiffness (N) of the adherend j
B_j	extensional and bending coupling stiffness (N.mm) of the adherend j
D_j	bending stiffness (N.mm ²) of the adherend j
E_j	Young's modulus (MPa) of the adherend j
E	Young's modulus (MPa) of in the adhesive
F	vector of forces
G	Coulomb's modulus (MPa) of the adhesive
G_j	Coulomb's modulus (MPa) of the adherend j
K	stiffness matrix

K_{BBa}	stiffness matrix of the Bonded-Bars element
K_{BBe}	stiffness matrix of the Bonded-Beams element
L	length (mm) of the overlap
M_j	moment (N.mm) in the adherend j around the z direction
N_j	force (N) in the adherend j in the x direction
Q_σ	nodal normal force (N) applied to the node σ in the x direction ($\sigma = i,j,k,l$)
R_σ	nodal shear force (N) applied to the node σ in the y direction ($\sigma = i,j,k,l$)
S_σ	nodal bending moment (N.mm) applied to the node σ around the z direction ($\sigma = i,j,k,l$)
S	adhesive peel stress (MPa)
T	adhesive shear stress (MPa)
U	vector of displacements
V_j	shear force (N) in the adherend j in the y direction
b	width (mm) of the adherends (lateral pitch between two rows of fasteners)
e	thickness (mm) of the adhesive
e_j	thickness (mm) of the adherend j
f	force (N) applied to the joint in the x direction
l_j	length (mm) of the beam outside the overlap of the adherend j
n	number of macro-elements
u_j	displacement (mm) of the adherend j in the x direction
u_a	displacement (mm) of the node a in the x direction ($a = i,j,k,l$)
w_j	displacement (mm) of the adherend j in the y direction
w_a	displacement (mm) of the node a in the y direction ($a = i,j,k,l$)
Δ	length (mm) of a macro-element
θ_j	angular displacement (rad) of the adherend j around the z direction
θ_a	angular displacement (rad) of the node a around the z direction ($a = i,j,k,l$)
(x,y,z)	direct orthonormal base

1. INTRODUCTION

1.1. Context

In the frame of the structural component design, bonding can be considered as a suitable assembly method or an attractive complement to conventional methods such as bolting or riveting. Bonding offers the possibility of joining without damaging various materials, like plastics or metals, as well as allowing for various combinations of materials. This first advantage is reinforced by a large choice of adhesive families and by the possibility to formulate adhesives, designed to best meet the joint specifications, while optimizing the structure. Bonding allows mainly for mass benefits with regard to other mechanical fastening methods, since the materials volume required is reduced to sustain static or fatigue loads. The Finite Element (FE) method could be able to address the stress analysis of bonded joints. Nevertheless, analyses based on FE models are mainly computationally cost expensive and it would be profitable to develop simplified approaches, enabling extensive parametric studies. The study, presented in this paper, takes place in this context. As highlighted in several literature surveys [1-3], a large number of simplified approaches for the stress analysis of bonded joints exist in the open literature.

1.2. Objective

The objective of this paper is to present a simplified approach for the stress analysis of bonded joints, taking into account an elasto-plastic adhesive material behavior. This topic was already addressed by several authors (e.g.: [4-11]), leading to the presentation of semi-analytical solutions. Indeed, in order to enlarge the application field of models, the number of simplifying hypotheses has to be restricted. The resolution of the complete set of governing equations, derived from the restricted hypotheses, requires then the development of dedicated procedures, even under the assumption of linear elastic

material behaviors. In this paper, a restricted number of simplifying hypotheses is similarly under consideration, so that closed-form solutions are not provided. However, an original procedure allowing for the resolution is presented. The simplified approach, presented in this paper, consists then in an iterative resolution scheme, using a simplified linear elastic method for the stress analysis of bonded joints. The simplified linear elastic method is based on the analytical formulation of a 4-node macro-element, in the frame of both 1D-bar and 1D-beam analyses. It is then exemplified on the single-lap bonded joint configuration (see Fig. 1 and Tab. 1).

1.3. Overview of the simplified linear elastic method

The simplified linear elastic method, originally presented in [12, 13], is inspired by the FE method and allows for the resolution of the set of governing differential equations. The displacements and forces in the adherends, as well as the adhesive stresses are then computed. The method consists in meshing the structure in elements. A full bonded overlap is meshed by a unique 4-node macro-element, which is specially formulated. This macro-element is called bonded-bars (BBa) or bonded-beams (BBe), depending on the 1D analysis frame. According to the classical FE rules, the stiffness matrix of the structure – termed K – is assembled and the selected boundary conditions are applied. The minimization of the total potential energy leads to find the vector of nodal displacements U such $F=KU$, where F is the vector of nodal forces. This approach based on macro-elements takes advantage of the flexibility of FE method. Indeed, by employing a macro-element as an elementary brick, it offers the possibility to simulate complex structures involving single-lap bonded joints [14]. Only simple manipulations on the stiffness matrix of the structure are required. An approach for the simulation of hybrid (bolted/bonded) joints can consist in employing macro-elements for the bonded parts and springs for the fasteners [12, 13]. Finally, various mechanical or thermal loadings could be taken into account, through the vector of nodal forces.

1.4. Overview of the paper

The mechanical and geometrical parameters are free; in particular, unbalanced configurations can be addressed. In the 1D-bar (1D-beam) frame, the adherends are simulated as linear elastic bars (as laminated linear elastic Euler-Bernoulli beams), while the adhesive layer simulation consists in continuously distributed linear or non-linear shear springs (in continuously distributed linear or non-linear shear and peeling springs). The adhesive layer thickness is assumed constant along the overlap.

BBa and BBe elements were previously developed [12, 13, 15]. Nevertheless, they do not take into account the shear stress in the adherends. The first part of the paper is then dedicated to the detailed presentation of the formulation of 1D-bar and 1D-beam macro-elements, including a linear variation of shear stress in the adherends, according to the approach of Tsai et al. [16]. Elements of validation are presented, by showing that under the same hypotheses as the Tsai et al. model, the same results are obtained. Secondly, the introduction of an iterative resolution scheme is presented, to take into account an elasto-plastic adhesive material behavior. The projection algorithm with elastic matrix is employed for the numerical resolution. Thirdly, a 1D-bar FE model, involving bar elements and shear springs, is developed as a numerical image of the simplified 1D-bar model. Besides, a plane stress (PS) and 3D FE models are developed to assess the performances of the simplified 1D-beam model.

2. LINEAR ELASTIC 1D-BAR AND 1D-BEAM MODELS

2.1. 1D-Bar model

2.1.1. Formulation of the BBa element

2.1.1.1 - Hypotheses. The model is based on the following hypotheses: (i) the thickness of the adhesive layer is constant along the overlap, (ii) the adherends are

linear elastic materials simulated as bars, (iii) the adhesive layer is simulated by an infinite number of linear elastic shear springs linking both adherends, and possibly (iv) the adherend shear stress varies linearly with the adherend thickness.

2.1.1.2. Governing Equations. The local equilibrium of both adherends (see Fig. 2) and the linear elastic material behaviors provide the following set of governing equations:

$$\begin{cases} \frac{dN_j}{dx} = (-1)^j bT \\ N_j = E_j b e_j \frac{du_j}{dx} \\ T = G \frac{u_2 - u_1}{e} \end{cases} \quad j = 1,2 \quad (1)$$

where e is the adhesive thickness, e_1 (e_2) the thickness of the adherend 1 (2), b the width, G the adhesive shear modulus, E_1 (E_2) the Young's modulus of the adherend 1 (2), N_1 (N_2) the normal force in the adherend 1 (2) and T is the adhesive shear stress. The displacements $u_1(x)$ ($u_2(x)$) are the normal displacements of points located at the abscissa x on the neutral line of adherend 1 (2) before deformation (see Fig. 3).

2.2.1.3. Stiffness matrix of the BBa element. The system of equations (1) leads to the following system of linear differential equations:

$$\begin{cases} \frac{d^2 u_1}{dx^2} + \frac{G}{e E_1 e_1} (u_2 - u_1) = 0 \\ \frac{d^2 u_2}{dx^2} + \frac{G}{e E_2 e_2} (u_2 - u_1) = 0 \end{cases} \quad (2)$$

The system of equations (2) is solved as:

$$\begin{cases} u_1 = 0.5 \left[-\theta (c_3 e^{-\eta x} + c_4 e^{\eta x}) + c_1 x + c_2 \right] \\ u_2 = 0.5 \left[\omega (c_3 e^{-\eta x} + c_4 e^{\eta x}) + c_1 x + c_2 \right] \end{cases} \text{ with: } \begin{cases} \theta = 1 + \frac{\psi}{\eta^2} \\ \omega = 1 - \frac{\psi}{\eta^2} \\ \psi = \frac{G}{e} \left(\frac{1}{e_1 E_1} - \frac{1}{e_2 E_2} \right) \\ \eta^2 = \frac{G}{e} \left(\frac{1}{e_2 E_2} + \frac{1}{e_1 E_1} \right) \end{cases} \quad (3)$$

where c_1 , c_2 , c_3 and c_4 are integration constants.

The boundary conditions at both extremities of the BBa element, in terms of displacements, lead to expressions for the integration constants, as functions of nodal displacements u_i , u_j , u_k and u_l (see Fig. 3):

$$\begin{cases} u_1(0) = u_i \\ u_2(0) = u_j \\ u_1(\Delta) = u_k \\ u_2(\Delta) = u_l \end{cases} \Rightarrow \begin{cases} c_1 = \frac{u_l \theta + u_k \omega - u_j \theta - u_i \omega}{\Delta} \\ c_2 = u_j \theta + u_i \omega \\ c_3 = \frac{(u_j - u_i) e^{\eta \Delta} - (u_l - u_k)}{2 \operatorname{sh}(\eta \Delta)} \\ c_4 = \frac{(u_l - u_k) - (u_j - u_i) e^{-\eta \Delta}}{2 \operatorname{sh}(\eta \Delta)} \end{cases} \quad (4)$$

where Δ is the length of the BBa element.

The linear elastic behavior of adherends allows then for the expression of adherend normal forces as a function of nodal displacements, through the integration constants (equation (1.1) and equation (3)):

$$\begin{cases} N_1 = 0.5 b E_1 e_1 \left[\theta \eta (c_1 e^{-\eta x} - c_2 e^{\eta x}) + c_3 \right] \\ N_2 = 0.5 b E_2 e_2 \left[\omega \eta (c_2 e^{\eta x} - c_1 e^{-\eta x}) + c_3 \right] \end{cases} \quad (5)$$

In the same way, the adhesive shear stress is then computed with equation (1.3) as:

$$T = 0.5 b E_1 e_1 \left[\theta \eta (c_1 e^{-\eta x} - c_2 e^{\eta x}) + c_3 \right] \quad (6)$$

The nodal forces Q_i, Q_j, Q_k, Q_l , which represent the action of nodes i, j, k, l respectively on the BBa element (see Fig. 3), can be expressed as functions of nodal displacements (equation (5)):

$$\begin{cases} Q_i = -N_1(0) \\ Q_j = -N_2(0) \\ Q_k = N_1(\Delta) \\ Q_l = N_2(\Delta) \end{cases} \Rightarrow \begin{cases} Q_i = -0.5 b E_1 e_1 [\theta \eta (c_1 - c_2) + c_3] \\ Q_j = -0.5 b E_2 e_2 [\omega \eta (c_2 - c_1) + c_3] \\ Q_k = 0.5 b E_1 e_1 [\theta \eta (c_1 e^{-\eta \Delta} - c_2 e^{\eta \Delta}) + c_3] \\ Q_l = 0.5 b E_2 e_2 [\omega \eta (c_2 e^{\eta \Delta} - c_1 e^{-\eta \Delta}) + c_3] \end{cases} \quad (7)$$

The stiffness matrix of the BBa element is defined by:

$$\begin{bmatrix} k_{ii} & k_{ij} & k_{ik} & k_{il} \\ k_{ji} & k_{jj} & k_{jk} & k_{jl} \\ k_{ki} & k_{kj} & k_{kk} & k_{kl} \\ k_{li} & k_{lj} & k_{lk} & k_{ll} \end{bmatrix} \begin{bmatrix} u_i \\ u_j \\ u_k \\ u_l \end{bmatrix} = \begin{bmatrix} Q_i \\ Q_j \\ Q_k \\ Q_l \end{bmatrix} \quad (8)$$

where:

$$k_{\sigma\tau} = \frac{\partial Q_\sigma}{\partial u_\tau}, \sigma, \tau = i, j, k, l \quad (9)$$

Finally, the stiffness matrix of the BBa element, named K_{BBa} , can be written as:

$$(10)$$

$$K_{BBa} = \omega \frac{E_2 e_2 b}{2\Delta} \begin{pmatrix} \frac{\eta\Delta}{th(\eta\Delta)} + \frac{E_1 e_1}{E_2 e_2} & 1 - \frac{\eta\Delta}{th(\eta\Delta)} & -\frac{\eta\Delta}{sh(\eta\Delta)} - \frac{E_1 e_1}{E_2 e_2} & \frac{\eta\Delta}{sh(\eta\Delta)} - 1 \\ 1 - \frac{\eta\Delta}{th(\eta\Delta)} & \frac{\eta\Delta}{th(\eta\Delta)} + \frac{E_2 e_2}{E_1 e_1} & \frac{\eta\Delta}{sh(\eta\Delta)} - 1 & -\frac{\eta\Delta}{sh(\eta\Delta)} - \frac{E_2 e_2}{E_1 e_1} \\ -\frac{\eta\Delta}{sh(\eta\Delta)} - \frac{E_1 e_1}{E_2 e_2} & \frac{\eta\Delta}{sh(\eta\Delta)} - 1 & \frac{\eta\Delta}{th(\eta\Delta)} + \frac{E_1 e_1}{E_2 e_2} & 1 - \frac{\eta\Delta}{th(\eta\Delta)} \\ \frac{\eta\Delta}{sh(\eta\Delta)} - 1 & -\frac{\eta\Delta}{sh(\eta\Delta)} - \frac{E_2 e_2}{E_1 e_1} & 1 - \frac{\eta\Delta}{th(\eta\Delta)} & \frac{\eta\Delta}{th(\eta\Delta)} + \frac{E_2 e_2}{E_1 e_1} \end{pmatrix}$$

2.1.1.4. *Considering the shear stress in the adherends.* Following [16], a linear distribution of the shear stress, named T_1 (T_2), in the thickness of the adherend 1 (2) is assumed:

$$T_j = -\frac{T}{2} \left(1 + (-1)^j 2 \frac{y_j}{e_j} \right), \quad j = 1, 2 \quad (11)$$

where y_1 and y_2 are local y-axis, as defined in Fig. 1.

The shear deformation, named γ_1 (γ_2), in the adherend 1 (2) is then given by:

$$\gamma_j = \frac{T_j}{G_j} = -\frac{1}{2} \left(1 + (-1)^j 2 \frac{y_j}{e_j} \right) \frac{T}{G_j} = \frac{\partial u_j(x, y_j)}{\partial y_j}, \quad j = 1, 2 \quad (12)$$

where G_1 (G_2) is the shear modulus of the adherend 1 (2).

The integration of equation (12) allows for the expression of the normal displacements of adherends, as functions of x and y_j :

$$u_j(x, y_j) = u_1(x, 0) + \int_0^{y_j} \frac{T_j}{G_j} dy_j \Rightarrow \begin{cases} u_1(x, y_1) = u_1(x, 0) + \frac{T}{2G_1} \left(\frac{y_1^2}{e_1} - y_1 \right) \\ u_2(x, y_2) = u_2(x, 0) - \frac{T}{2G_2} \left(\frac{y_2^2}{e_2} + y_2 \right) \end{cases} \quad (13)$$

The normal forces in the adherends are then deduced:

$$N_j = b \int_{-\frac{e_j}{2}}^{\frac{e_j}{2}} E_j \frac{\partial u_j(x, y_j)}{\partial x} dy_j \Rightarrow \begin{cases} N_1 = be_1 E_1 \left(\frac{du_1(x,0)}{dx} - \frac{1}{3} \frac{e_1}{G_2} \frac{dT}{dx} \right) \\ N_2 = be_2 E_2 \left(\frac{du_2(x,0)}{dx} + \frac{1}{3} \frac{e_1}{G_2} \frac{dT}{dx} \right) \end{cases} \quad (14)$$

But, by noticing that the average value of the normal displacement on the adherend thickness is given by:

$$\bar{u}_j = \frac{1}{e_j} \int_{-\frac{e_j}{2}}^{\frac{e_j}{2}} u_j(x, y_j) dy_j \Rightarrow \begin{cases} \bar{u}_1 = u_1(x,0) - \frac{1}{3} e_1 \frac{T}{G_1} \\ \bar{u}_2 = u_2(x,0) + \frac{1}{3} e_2 \frac{T}{G_2} \end{cases} \quad (15)$$

the normal forces in the adherends and the adhesive shear stress can be written as:

$$\begin{cases} N_j = be_j E_j \frac{d\bar{u}_j}{dx} \\ T = \bar{G} \frac{\bar{u}_2 - \bar{u}_1}{e} \end{cases} \text{ with } \begin{cases} \bar{G} = \frac{G}{1 + \xi^2} \\ \xi^2 = \frac{1}{3} \frac{G}{e} \left(\frac{e_1}{G_1} + \frac{e_2}{G_2} \right) \end{cases} \quad (16)$$

Finally, to take into account a linear variation of the shear stress in the adherends, the resolution consists in substituting G by \bar{G} and u_j by \bar{u}_j , in the formulation, which does not consider any shear stress in the adherends.

2.1.2. Assembly and validation on the exemplified single-lap joint. The single-lap bonded joint is meshed as following: (i) the overlap is meshed which 1 BBa element, (ii) each adherend outside the overlap is meshed with 1 bar element. This mesh leads to a total number of 6 nodes (see Fig. 4).

The stiffness matrix of the single-lap joint is then assembled, according to the classical FE rules, through the stiffness matrices of each element. The stiffness matrix for the bar element, named K_{bar} , is:

$$K_{bar} = \frac{E_j e_j b}{l_j} \begin{pmatrix} 1 & -1 \\ -1 & 1 \end{pmatrix}, \quad j = 1,2 \quad (17)$$

where l_1 (l_2) is the length of the bar outside the overlap of the adherend 1 (2).

Following the classical FE rules, the boundary conditions are then applied to the single-lap bonded joint, which is clamped at one extremity and free to move at the other one, where a force $f=10$ N is applied (see Fig. 4). A total number of degrees of freedom (DoF) equal to 5 is then involved. The resolution consists then in inverting a 5x5 linear system. The adhesive stress distribution predicted by [16] is compared to the model predictions for the single-lap bonded joint defined in Fig. 1 and Tab. 1. The superimposition of curves shown in Fig. 5, allows for the conclusion that the same hypotheses lead to the same results.

2.2. 1D-beam model

2.2.1. Formulation of the BBe element

2.2.1.1. Hypotheses. The model is based on the following hypotheses: (i) the thickness of the adhesive layer is constant along the overlap, (ii) the adherends are simulated by linear elastic Euler-Bernoulli laminated beams, (iii) the adhesive layer is simulated by an infinite number of elastic shear and transverse springs linking both adherends, and possibly (iv), the adherend shear stress varies linearly with the adherend thickness.

2.2.1.2. *Governing equations.* The local equilibrium of both adherends (see Fig. 6) leads to the following system of six equations:

$$\begin{cases} \frac{dN_j}{bdx} = (-1)^j T \\ \frac{dV_j}{bdx} = (-1)^{j+1} S \\ \frac{dM_j}{dx} + V_j + \frac{e_j}{2} bT = 0 \end{cases}, \quad j = 1,2 \quad (18)$$

where S is the adhesive peeling stress, V_1 (V_2) the shear force in the adherend 1 (2) and M_1 (M_2) the bending moment in the adherend 1 (2).

This local equilibrium is the one derived and employed by Goland and Reissner [17] in their classical theory. Furthermore, considering a possible extensional and bending coupling stiffness in the adherends, the constitutive equations are expressed as:

$$\begin{cases} N_j = A_j \frac{du_j}{dx} - B_j \frac{d^2w_j}{dx^2} \\ M_j = -B_j \frac{du_j}{dx} + D_j \frac{d^2w_j}{dx^2}, \quad j = 1,2 \\ \theta_j = \frac{dw_j}{dx} \end{cases} \quad (19)$$

with A_j the extensional stiffness, B_j the coupling stiffness, and D_j the bending stiffness.

It is assumed that $\Delta_j = A_j^2 - B_j D_j$ is not equal to zero. The adhesive is considered as linear elastic and is simulated by an infinite number of shear and transverse normal springs. The adhesive shear stress and the adhesive peeling stress are then expressed by:

$$\begin{cases} T = G \frac{u_2 - u_1 - \frac{1}{2} e_1 \theta_1 - \frac{1}{2} e_2 \theta_2}{e} \\ S = E \frac{w_1 - w_2}{e} \end{cases} \quad (20)$$

where E is the Young's modulus of the adhesive, w_1 (w_2) the deflection of the adherend 1 (2) and θ_1 (θ_2) the bending angle of the adherend 1 (2).

2.2.1.3. Stiffness Matrix of the BBe element.

System of differential equations in terms of adhesive stresses. The equation (19) is written as:

$$\begin{cases} \frac{du_j}{dx} = \frac{D_j N_j + B_j M_j}{\Delta_j} \\ \frac{d^2 w_j}{dx^2} = \frac{A_j M_j + B_j N_j}{\Delta_j} \end{cases}, j = 1, 2 \quad (21)$$

By combining equations (18), (20), (21), the following linear differential equation system, in terms of adhesive stresses, is obtained:

$$\begin{cases} \frac{d^3 T}{dx^3} = k_1 \frac{dT}{dx} + k_2 S \\ \frac{d^4 S}{dx^4} = -k_4 S - k_3 \frac{dT}{dx} \end{cases} \quad (22)$$

where:

$$\begin{cases} k_1 = \frac{Gb}{e} \left[\frac{D_1}{\Delta_1} \left(1 + \frac{A_1 e_1^2}{4D_1} \right) + \frac{D_2}{\Delta_2} \left(1 + \frac{A_2 e_2^2}{4D_2} \right) + \left(\frac{e_1 B_1}{\Delta_1} - \frac{e_2 B_2}{\Delta_2} \right) \right] \\ k_2 = \frac{Gb}{e} \left[\frac{e_1 A_1}{2\Delta_1} - \frac{e_2 A_2}{2\Delta_2} + \left(\frac{B_1}{\Delta_1} + \frac{B_2}{\Delta_2} \right) \right] \\ k_3 = \frac{Eb}{e} \left[\frac{e_1 A_1}{2\Delta_1} - \frac{e_2 A_2}{2\Delta_2} + \left(\frac{B_1}{\Delta_1} + \frac{B_2}{\Delta_2} \right) \right] \\ k_4 = \frac{Eb}{e} \left[\frac{A_1}{\Delta_1} + \frac{A_2}{\Delta_2} \right] \end{cases} \quad (23)$$

The system of differential equations (22) can be uncoupled by differentiation and linear combination as:

$$\begin{cases} \frac{d^6 S}{dx^6} - k_1 \frac{d^4 S}{dx^4} + k_4 \frac{d^2 S}{dx^2} + S(k_2 k_3 - k_1 k_4) = 0 \\ \frac{d}{dx} \left(\frac{d^6 T}{dx^6} - k_1 \frac{d^4 T}{dx^4} + k_4 \frac{d^2 T}{dx^2} + T(k_2 k_3 - k_1 k_4) \right) = 0 \end{cases} \quad (24)$$

This system is solved and the adhesive shear and peeling stresses are thus written as (see Appendix A):

$$\begin{cases} S(x) = \left[\begin{aligned} & \overline{K}_1 e^{sx} \sin(tx) + \overline{K}_2 e^{sx} \cos(tx) + \overline{K}_3 e^{-sx} \sin(tx) \\ & + \overline{K}_4 e^{-sx} \cos(tx) + \overline{K}_5 e^{rx} + \overline{K}_6 e^{-rx} \end{aligned} \right] \\ T(x) = \left[\begin{aligned} & K_1 e^{sx} \sin(tx) + K_2 e^{sx} \cos(tx) + K_3 e^{-sx} \sin(tx) \\ & + K_4 e^{-sx} \cos(tx) + K_5 e^{rx} + K_6 e^{-rx} + K_7 \end{aligned} \right] \end{cases} \quad (25)$$

There are then 13 integration constants. However, by introducing these previous expressions of adhesive stresses in equation (22), the integration constants of the adhesive peeling stress appear linked to those of adhesive shear stress as:

$$\left\{ \begin{array}{l}
\overline{K_1} = \frac{s(s^2 - 3t^2 - k_1)}{k_2} K_1 + \frac{t(t^2 - 3s^2 + k_1)}{k_2} K_2 = \alpha_1 K_1 + \alpha_2 K_2 \\
\overline{K_2} = \frac{t(3s^2 - t^2 - k_1)}{k_2} K_1 + \frac{s(s^2 - 3t^2 - k_1)}{k_2} K_2 = -\alpha_2 K_1 + \alpha_1 K_2 \\
\overline{K_3} = \frac{s(3t^2 - s^2 + k_1)}{k_2} K_3 + \frac{t(t^2 - 3s^2 + k_1)}{k_2} K_4 = -\alpha_1 K_3 + \alpha_2 K_4 \\
\overline{K_4} = \frac{t(3s^2 - t^2 - k_1)}{k_2} K_3 + \frac{s(3t^2 - s^2 + k_1)}{k_2} K_4 = -\alpha_2 K_3 - \alpha_1 K_4 \\
\overline{K_5} = \frac{r(r^2 - k_1)}{k_2} K_5 = \alpha_3 K_5 \\
\overline{K_6} = \frac{r(k_1 - r^2)}{k_2} K_6 = -\alpha_3 K_6
\end{array} \right. \quad (26)$$

Finally, 7 independent integration constants are remaining: K_1 to K_7 .

Nodal displacements and forces. The determination of the stiffness matrix of BBe element requires the determination of nodal displacements and forces (see Fig. 7). Following the resolution scheme in [18], the idea is to express the displacements and the forces in the adherends, as a function of the stress adhesives and of their derivatives. The computation is fully detailed in Appendix B. It is shown that a total number of 12 integration constants is finally involved: K_1 to K_7 , J_1 to J_3 and J_5 to J_6 . The displacements in the adherends are then expressed as:

$$\left\{ \begin{array}{l}
u_1(x) = \tilde{\beta}_1 T + \overline{\beta}_1 \frac{dS}{dx} - \frac{b\Delta^2 K_7 - 6B_1 J_0 / \Delta}{2A_1} \left(\frac{x}{\Delta} \right)^2 + J_5 \frac{x}{\Delta} + J_6 \\
u_2(x) = \tilde{\beta}_2 T + \overline{\beta}_2 \frac{dS}{dx} + \frac{b\Delta^2 K_7 + 6B_2 J_0 / \Delta}{2A_2} \left(\frac{x}{\Delta} \right)^2 + \left(J_5 + \frac{J_1}{\Delta} (e_1 + e_2) \right) \frac{x}{\Delta} \\
\quad + J_6 + \frac{J_2}{2\Delta} (e_1 + e_2) - K_7 \left(\frac{e_1}{2} \tilde{\beta}_5 + \frac{e_2}{2} \tilde{\beta}_6 \right) \\
w_1(x) = \tilde{\beta}_3 \left(k_4 \frac{dT}{dx} + k_2 \frac{d^2 S}{dx^2} \right) + \overline{\beta}_5 S + J_0 \left(\frac{x}{\Delta} \right)^3 + J_1 \left(\frac{x}{\Delta} \right)^2 + J_2 \frac{x}{\Delta} + J_3 \\
w_2(x) = \tilde{\beta}_4 \left(k_4 \frac{dT}{dx} + k_2 \frac{d^2 S}{dx^2} \right) + \overline{\beta}_6 S + J_0 \left(\frac{x}{\Delta} \right)^3 + J_1 \left(\frac{x}{\Delta} \right)^2 + J_2 \frac{x}{\Delta} + J_3 \\
\theta_1(x) = \tilde{\beta}_5 T + \overline{\beta}_5 \frac{dS}{dx} + 3J_0 \frac{x^2}{\Delta^3} + 2J_1 \frac{x}{\Delta^2} + \frac{J_2}{\Delta} - K_7 \tilde{\beta}_5 \\
\theta_2(x) = \tilde{\beta}_6 T + \overline{\beta}_6 \frac{dS}{dx} + 3J_0 \frac{x^2}{\Delta^3} + 2J_1 \frac{x}{\Delta^2} + \frac{J_2}{\Delta} - K_7 \tilde{\beta}_6
\end{array} \right. \quad (27)$$

The nodal displacements are then the values in $x=0$ and $x=\Delta$ of equation (27). The constitutive equations (19) allow for the computation of normal and shear forces and of bending moments in both adherends:

$$\left\{ \begin{array}{l}
N_1(x) = \tilde{a}_1 \frac{dT}{dx} + \overline{a}_1 \frac{d^2 S}{dx^2} - bK_7 x - 2B_1 \frac{J_1}{L^2} + A_1 \frac{J_5}{L} \\
N_2(x) = \tilde{a}_2 \frac{dT}{dx} + \overline{a}_2 \frac{d^2 S}{dx^2} + bK_7 x + J_1 \left(-\frac{2B_2}{L^2} + A_2 \frac{e_1 + e_2}{L^2} \right) + A_2 \frac{J_5}{L} \\
M_1(x) = \tilde{a}_3 \frac{dT}{dx} + \overline{a}_3 \frac{d^2 S}{dx^2} + \frac{x}{L} \left(\frac{6J_0}{L^2} \frac{\Delta_1}{A_1} + bLK_7 \frac{B_1}{A_1} \right) + 2D_1 \frac{J_1}{L^2} - B_1 \frac{J_5}{L} \\
M_2(x) = \tilde{a}_4 \frac{dT}{dx} + \overline{a}_4 \frac{d^2 S}{dx^2} + \frac{x}{L} \left(\frac{6J_0}{L^2} \frac{\Delta_2}{A_2} - bLK_7 \frac{B_2}{A_2} \right) + J_1 \left(\frac{2D_2}{L^2} - B_2 \frac{e_1 + e_2}{L^2} \right) - B_2 \frac{J_5}{L} \\
V_1(x) = -\tilde{a}_3 \frac{d^2 T}{dx^2} - \overline{a}_3 \frac{d^3 S}{dx^3} - \frac{1}{L} \left(\frac{6J_0}{L^2} \frac{\Delta_1}{A_1} + bLK_7 \frac{B_1}{A_1} \right) - \frac{e_1 b}{2} T \\
V_2(x) = -\tilde{a}_4 \frac{d^2 T}{dx^2} - \overline{a}_4 \frac{d^3 S}{dx^3} - \frac{1}{L} \left(\frac{6J_0}{L^2} \frac{\Delta_2}{A_2} - bLK_7 \frac{B_2}{A_2} \right) - \frac{e_2 b}{2} T
\end{array} \right. \quad (28)$$

The nodal forces are then the values in $x=0$ and $x=\Delta$ of equation (28).

Stiffness matrix. The coefficients of the stiffness matrix of the BBe element are obtained by differentiating each nodal force by each nodal displacement:

$$K_{BBe} = \begin{pmatrix} \left[\frac{\partial Q_\sigma}{\partial u_\tau} \right] & \left[\frac{\partial Q_\sigma}{\partial w_\tau} \right] & \left[\frac{\partial Q_\sigma}{\partial \theta_\tau} \right] \\ \left[\frac{\partial R_\sigma}{\partial u_\tau} \right] & \left[\frac{\partial R_\sigma}{\partial w_\tau} \right] & \left[\frac{\partial R_\sigma}{\partial \theta_\tau} \right] \\ \left[\frac{\partial S_\sigma}{\partial u_\tau} \right] & \left[\frac{\partial S_\sigma}{\partial w_\tau} \right] & \left[\frac{\partial S_\sigma}{\partial \theta_\tau} \right] \end{pmatrix}, \sigma, \tau = i, j, k, l \quad (29)$$

where Q_σ (R_σ) is the nodal normal (shear) forces and S_σ are the nodal bending moments.

The 12 nodal displacements ($u_\gamma, \gamma = 1:12$) and the 12 nodal forces ($Q_\alpha, \alpha = 1:12$) are expressed as functions of the 12 independent integration constants ($C_\beta, \beta = 1:12$). The nodal forces depend linearly on integration constants, as well as the nodal displacements. Thus, the integration constants depend linearly on the nodal displacements (equation (30)), enabling the determination of 144 coefficients of K_{BB} (equation (31)):

$$Q_\alpha = \sum_{\beta=1}^{12} n_{\alpha\beta} C_\beta \quad \text{and} \quad C_\beta = \sum_{\gamma=1}^{12} m'_{\beta\gamma} u_\gamma \quad (30)$$

$$\frac{\partial Q_\alpha}{\partial u_\delta} = \sum n_{\alpha\beta} \sum m'_{\beta\gamma} \frac{\partial u_\gamma}{\partial u_\delta} \quad (31)$$

But:

$$\frac{\partial u_\gamma}{\partial u_\delta} = \delta_{\gamma\delta} = \begin{cases} 1 & \text{if } \gamma = \delta \\ 0 & \text{if } \gamma \neq \delta \end{cases} \Rightarrow \frac{\partial Q_\alpha}{\partial u_\delta} = \sum_{\beta=1}^{12} n_{\alpha\beta} m'_{\beta\delta} \quad (32)$$

$$m'_{\beta\delta} = C_\beta(u_\delta = 1, u_{\gamma \neq \delta} = 0) = C_\beta(0, \dots, 0, u_\delta = 1, 0, \dots, 0)$$

The coefficients of K_{BB} are thus obtained through:

$$[K_{BB}]_{\alpha,\delta} = \frac{\partial Q_\alpha}{\partial u_\delta} = \sum_{\beta=1}^{12} n_{\alpha\beta} C_\beta(0 \dots 0, u_\delta = 1, 0 \dots 0) \quad (33)$$

Practically, $C_{\beta}(0...0, u_{\delta}=1, 0...0)$ is automatically generated by looping on the 12 canonical vectors of displacement, through the following inversion $C_{\beta}[(0...0, u_{\delta}=1, 0...0)] = M^{-1}(0...0, u_{\delta}=1, 0...0)$.

2.2.1.4. *Considering the shear stress in the adherends.* This section describes how to consider the shear effects in the adherends by simply adapting a finite number of previous parameters. The approach is based on the assumption of a linear variation of shear stresses in the adherends, according to Tsai et al. theory [16]. From equations (11), the shear strain γ_1 for the upper adherend and γ_2 for the lower one are expressed as:

$$\gamma_j = \frac{T_j}{G_j} = -\frac{1}{2} \left(1 + (-1)^j 2 \frac{y_j}{e_j} \right) \frac{T}{G_j} = \frac{\partial u_j(x, y_j)}{\partial y_j} + \frac{dw_j}{dx}, \quad j = 1, 2 \quad (34)$$

The integration of normal displacements with respect dy_j provides:

$$\begin{cases} u_1(x, y_1) = u_1(x, 0) - \frac{T}{2G_1} \left[y_1 - \frac{y_1^2}{e_1} \right] - y_1 \frac{dw_1}{dx} \\ u_2(x, y_2) = u_2(x, 0) - \frac{T}{2G_2} \left[y_2 + \frac{y_2^2}{e_2} \right] - y_2 \frac{dw_2}{dx} \end{cases} \quad (35)$$

Taking into account the previous shape of normal displacements, the constitutive equations of adherends (19) become:

$$\left\{ \begin{array}{l}
N_1 = A_1 \frac{du_1}{dx} - B_1 \frac{d^2w_1}{dx^2} - C_1 \frac{dT}{dx} \\
N_2 = A_2 \frac{du_2}{dx} - B_2 \frac{d^2w_2}{dx^2} - C_2 \frac{dT}{dx} \\
M_1 = -B_1 \frac{du_1}{dx} + D_1 \frac{d^2w_1}{dx^2} + C'_1 \frac{dT}{dx} \\
M_2 = -B_2 \frac{du_2}{dx} + D_2 \frac{d^2w_2}{dx^2} + C'_2 \frac{dT}{dx} \\
C_1 = \frac{e_1 B_1 - D_1}{2e_1 G_1} \\
C_2 = \frac{e_2 B_2 + D_2}{2e_2 G_2} \\
C'_1 = \frac{e_1 D_1 - F_1}{2e_1 G_1} \\
C'_2 = \frac{e_2 D_2 + F_2}{2e_2 G_2}
\end{array} \right. \quad (36)$$

with:

$$F_j = \frac{b}{4} \sum_{p_j=1}^{n_j} Q_j^{p_j} [h_{p_j}^4 - h_{p_j-1}^4] \quad , \quad j = 1,2 \quad (37)$$

where h_{p_i} the y-coordinates of the p_j^{th} layer, and $Q_j^{p_i}$ the reduced rigidity matrix of the p^{th} ply of adherends j .

As detailed in Appendix C, the modification of the shape of the constitutive equations of adherends results in modification of suitable constants only.

2.3.2. Assembly and validation on the exemplified single-lap joint. The single-lap bonded joint is meshed as following: (i) the overlap is meshed which 1 BBe element, (ii) each adherend outside the overlap is meshed with 1 bar element. This mesh leads to a total number of 6 nodes (see Fig. 8).

The stiffness matrix of the single-lap joint is then assembled, according to the classical FE rules, from the stiffness matrix of each element. The stiffness matrix of a beam element, named K_{beam} , is written (according to [15]):

$$K_{beam} = \begin{pmatrix} \frac{A_j}{l_j} & -\frac{A_j}{l_j} & 0 & 0 & -\frac{B_j}{l_j} & \frac{B_j}{l_j} \\ -\frac{A_j}{l_j} & \frac{A_j}{l_j} & 0 & 0 & \frac{B_j}{l_j} & -\frac{B_j}{l_j} \\ 0 & 0 & \frac{12}{l_j^3} \frac{\Delta}{A_j} & -\frac{12}{l_j^3} \frac{\Delta}{A_j} & \frac{6}{l_j^2} \frac{\Delta}{A_j} & \frac{6}{l_j^2} \frac{\Delta}{A_j} \\ 0 & 0 & -\frac{12}{l_j^3} \frac{\Delta}{A_j} & \frac{12}{l_j^3} \frac{\Delta}{A_j} & -\frac{6}{l_j^2} \frac{\Delta}{A_j} & -\frac{6}{l_j^2} \frac{\Delta}{A_j} \\ -\frac{B_j}{l_j} & \frac{B_j}{l_j} & \frac{6}{l_j^2} \frac{\Delta}{A_j} & -\frac{6}{l_j^2} \frac{\Delta}{A_j} & \frac{1}{l_j} \left(3 \frac{\Delta}{A_j} + D_j \right) & \frac{1}{l_j} \left(3 \frac{\Delta}{A_j} - D_j \right) \\ \frac{B_j}{l_j} & -\frac{B_j}{l_j} & \frac{6}{l_j^2} \frac{\Delta}{A_j} & -\frac{6}{l_j^2} \frac{\Delta}{A_j} & \frac{1}{l_j} \left(3 \frac{\Delta}{A_j} - D_j \right) & \frac{1}{l_j} \left(3 \frac{\Delta}{A_j} + D_j \right) \end{pmatrix}, \quad j = 1,2 \quad (38)$$

Following the classical FE rules, the boundary conditions are then applied to the single-lap bonded joint, which is simply supported at both extremities, fixed according to the x-axis at one extremity and free at the other one, where a force $f=10$ N is applied (see Fig. 8). A total number of DoF equal to 15 is then involved. The resolution consists then in inverting a 15x15 linear system.

The adhesive stress distribution predicted by [16] is compared to the present model predictions for the single-lap bonded joint defined in Fig. 1 and Tab. 1. In order to perform a comparison on exactly the same hypotheses, the length outside the overlap is computed according to the Goland and Reissner theory [17], resulting in a same bending moment at both overlap ends (for a beam approach) under the applied force ($l_i=91$ mm). Moreover, the factors C'_j are set to zero. The superimposition of curves shown in Fig. 9 allows for the conclusion that the same hypotheses lead to the same results.

3. ASSUMING AN ELASTO-PLASTIC ADHESIVE MATERIAL

3.1. Numerical approach

In this section, the adhesive, employed in the bonded area, is assumed to have an elasto-plastic behavior. To take into account this non-linear behavior, an iterative

procedure [19] is implemented, starting from the previous linear elastic formulation. This iterative procedure is illustrated in Fig. 10, for a stress step resulting in a current elastic stress state characterized by an equivalent stress superior to the yield stress. This current elastic stress state is obtained through the linear computation $F=KU$, representing the first step of the procedure. The second step corresponds to the projection of the equivalent stress to the elastic stress state on the yield function, allowing for the computation for a first residue R , relevant to the difference between the elastic stress state and the projected stress state. In this paper, this second step is presented assuming an elastic perfectly plastic behavior. The third step consists in imposing to the structure the residue, such $R=KU$. This procedure is repeated, while the norm of the residue is higher than a prescribed threshold. The residues have thus to be computed. Hereafter, the equivalent stress chosen for the 1D-bar model is the shear stress (maximal stress criterion), while for the 1D-beam model, the criterion is the Von Mises equivalent stress.

3.2. Example of application for structures: single-lap joint, in-plane loading

3.2.1. *Equilibrium of the structure.* For both 1D-bar and 1D-beam models, the equilibrium of the structure is such that at any abscissa along the overlap the sum of normal and shear forces in the adherends is constant:

$$\begin{aligned} N_1 + N_2 = N_2(L) = N_1(0) = f \\ V_1 + V_2 = V_2(L) = V_1(0) \end{aligned} \tag{39}$$

For both 1D-bar and 1D-beam models, the local equilibrium of adherends, according to the x-axis and y-axis, allows for a relationship between the normal and shear forces in the adherends and the adhesive shear and peeling stresses:

$$\begin{aligned}
N_2(x) - N_2(0) &= N_2(x) = b \int_0^x T dx \\
V_2(x) - V_2(0) &= V_2(x) = b \int_0^x S dx
\end{aligned}
\tag{40}$$

In particular, the area under the shear stress distribution along the overlap (named S_0) multiplied by the overlap width is equal to the applied force:

$$S_0 = b \int_0^L T(x) dx = f
\tag{41}$$

This last equilibrium requirement is used in the iterative procedure to ensure its convergence.

3.2.2. Determination of the nodal residue.

3.2.2.1. *Case with a mesh with n -macro-elements.* The bonded overlap is regularly meshed in n macro-elements, such $n\Delta=L$ (see Fig. 11). A total number of $2n+2$ nodes is involved.

For 1D-bar case. The elastic shear stress on the k^{th} node is computed through the nodal displacements and is quoted $T_e(k)$. The projected stress on the yield function is named $T_p(k)$. The difference between these two stresses is named $\delta T(k)$:

$$\forall k \in [2; 2n+3], \quad \delta T(k) = T_e(k) - T_p(k)
\tag{42}$$

Along the elastic zones, this difference is equal to zero. Moreover, this difference is the same for both nodes located at the same abscissa:

$$\forall k \in [2; 2n + 3], \forall p \in [1; n + 1], \quad \delta \hat{T}(p) = \delta T(k = 2p) = \delta T(k = 2p + 1) \quad (43)$$

Before the application of the prescribed displacements, the relevant components of the residue vector to normal nodal forces are such:

$$\begin{aligned} R(0) &= 0 \\ \text{for } p \in [1; n + 1], \quad &\begin{cases} R(2p) = -b\Delta\delta \hat{T}(p) \\ R(2p + 1) = b\Delta\delta \hat{T}(p) \end{cases} \\ R(2n + 4) &= f \end{aligned} \quad (44)$$

For 1D-beam case. The elastic shear and peeling stresses on the k^{th} node are computed through the nodal displacements and are named $T_e(k)$ and $S_e(k)$, respectively. The projected shear and peeling stresses on the yield function are named $T_p(k)$ and $S_p(k)$, respectively. As for the 1D-bar case, the difference between the elastic peeling stress and the projected peeling stress is such:

$$\forall k \in [2; 2n + 3], \forall p \in [1; n + 1], \quad \delta \hat{S}(p) = \delta S(k = 2p) = \delta S(k = 2p + 1) = S_e(k) - S_p(k) \quad (45)$$

Before the application of the prescribed displacements, the relevant components of the residue vector to normal nodal forces are given in equation (44), whereas those relevant to the shear nodal forces are such:

$$\begin{aligned} R(0) &= 0 \\ \text{for } p \in [1; n + 1], \quad &\begin{cases} R(2p) = -b\Delta\delta \hat{S}(p) \\ R(2p + 1) = b\Delta\delta \hat{S}(p) \end{cases} \\ R(2n + 4) &= 0 \end{aligned} \quad (46)$$

3.2.2.2. Case with a mesh with one macro-element. The bonded overlap is meshed with one macro-element only, which implies a total number of six nodes (see Fig. 5).

For the 1D-bar case. The elastic shear stress is computed at any abscissa x with equation (6) and is named $T_e(x)$. The projected stress on the yield function is named $T_p(x)$. The difference between these two stresses is named $\delta T(x)$. The residue is obtained after summation of $\delta T(x)$ for any abscissa such $\delta T(x) \neq 0$. More precisely, if the elastic zone is included between x_1 and x_2 (see Fig. 12), before the application of the prescribed displacements, the components of the residue vector are:

$$\begin{cases}
 R(0) = 0 \\
 R(2) = -b \int_0^{x_1} \delta T(x) dx \\
 R(3) = b \int_0^{x_1} \delta T(x) dx \\
 R(4) = -b \int_0^L \delta T(x) dx \\
 R(5) = b \int_0^L \delta T(x) dx \\
 R(6) = f
 \end{cases} \quad (47)$$

For the 1D-beam case. The elastic shear stress and peeling stresses are computed at any abscissa x with equation (25) and are named $T_e(x)$ and $S_e(x)$, respectively. The projected shear and peeling stresses on the yield function are named $T_p(x)$ and $S_p(x)$. The difference between the elastic and projected shear and peeling stresses are named $\delta T(x)$ and $\delta S(x)$. The relevant components of residue vector to normal nodal forces are the same as that given in equation (47). In the same way, before the application of the prescribed displacements, the relevant components of residue vector to shear nodal forces are such:

$$\begin{cases}
R(0) = 0 \\
R(2) = -b \int_0^{x1} \delta S(x) dx \\
R(3) = b \int_0^{x1} \delta S(x) dx \\
R(4) = -b \int_0^L \delta S(x) dx \\
R(5) = b \int_0^L \delta S(x) dx \\
R(6) = 0
\end{cases} \quad (48)$$

3.2.3. *Projected stresses.* In the 1D-bar model, only one adhesive stress component is involved. The projected stress depends only on the yield function following the maximal stress criterion. In the 1D-beam model, the peeling stress and the shear stress are considered, allowing the computation of the Von Mises equivalent stress, named σ_e , which is chosen as yield criterion:

$$\sigma_e = \sqrt{3T_e^2 + S_e^2} \quad (49)$$

The equivalent projected stress, named σ_p , is computed as a function of T_p and S_p as:

$$\sigma_p = \sqrt{3T_p^2 + S_p^2} \quad (50)$$

When the yield criterion is exceeded, the equivalent stress is expressed as:

$$3T_e^2 + S_e^2 = \sigma_p^2 + Q^2 \quad (51)$$

where Q characterizes the exceeding of yield criterion.

The equation (51) can be rearranged as:

$$\sigma_p^2 = 3T_e^2 + S_e^2 - \frac{3T_e^2 + S_e^2}{3T_e^2 + S_e^2} Q^2 \quad (52)$$

leading to:

$$\sigma_p^2 = 3 \left(T_e^2 - \frac{T_e^2}{3T_e^2 + S_e^2} Q^2 \right) + \left(S_e^2 - \frac{S_e^2}{3T_e^2 + S_e^2} Q^2 \right)^2 \quad (53)$$

Finally, the projected stresses are written as functions of the elastic stresses and yield criterion excess:

$$\begin{cases} T_p = \text{sign}(T_e) T_e \sqrt{1 - \frac{Q^2}{3T_e^2 + S_e^2}} \\ S_p = \text{sign}(S_e) S_e \sqrt{1 - \frac{Q^2}{3T_e^2 + S_e^2}} \end{cases} \quad (54)$$

3.2.4. Solution procedure. The solution procedure is summarized hereafter.

A. Linear elastic computation

A.1 the stiffness matrix of the structure is computed (see section 2)

A.2 initialization of variables:

- $f_R = f$
- $R = F$, such ${}^tF = (0 \dots 0 f)$

A.3 computation of $U = K^{-1}R$, after applying the boundary conditions in displacement

A.4 computation of adhesive elastic stresses for any abscissa of overlap (see section 2)

A.5 computation of adhesive equivalent stress σ_e

A.6 computation of S_0 (see section 3.2.1)

B. Yielding test

if σ_e is inferior to the adhesive yield stress then end

else computation of Q as the difference of the adhesive equivalent stress and the adhesive yield stress

C. *Plastic loop*

C.1 projection of adhesive stresses on the yield function (see section 3.2.3)

C.2 computation of the difference between the adhesive elastic stresses and the adhesive projected stress (see section 3.2.2)

C.3 update of R (see section 3.2.2)

C.4 if $norm(R) < threshold_2$ then go to D else go to A.3

D. *Global equilibrium*

if $abs(S_0 - f) > threshold_2$ then $f_R = f_R - (S_0 - f)$ and go to A.3

else end

4. COMPARISON WITH FINITE ELEMENT PREDICTIONS

4.1. Overview

In order to assess and to validate both models based on a simplified approach, FE models are developed using SAMCEF FE code v14-1. For validation purposes, a 1D-bar FE model is compared to the current 1D-bar model, without considering any shear deformations in the adherends. For assessment, a PS and a 3D FE model are compared with the current 1D-beam model, including a linear variation of the shear stress in the adherends. The joint is clamped at one end and free to move at the other end in the longitudinal direction only, where the load is applied. A force per unit of width unit of 10 N.mm^{-1} is applied. The geometry of the single lap joint is that introduced in Fig. 1 and Tab. 1. For the 3D FE model, the width of structure is taken equal to 1 mm. The adherends are assumed to be linear elastic and the material characteristics are given in Tab. 1. The adhesive is considered as elastic perfectly plastic. The adhesive elastic parameters are given in Tab.

1. In the 1D-bar analysis, the adhesive remains in its elastic domain if the shear stress is inferior to 0.55 MPa. For all the others analyses, the Von Mises yield criterion is employed with a yield stress of 1.6 MPa. The FE computations are geometrically linear. 100 macro-elements are employed in the models based on the simplified approaches. It is indicated (not discussed here) that a mesh with 1 macro-element lead to almost the same results for all the cases tested. For the PS and 3D FE models, the stresses are measured along the middle line of the adhesive layer and in the symmetry plane for the 3D FE model. Indeed, in contrast to refined PS or 3D FE models [20], the models based on the simplified approach are not able to capture the edge effects at the interfaces with the adherends or at the free edges.

4.2. Description of FE models

4.2.1. 1D-bar FE model. The adherends are simulated by beam elements (SAMCEF type T022). The adhesive layer is simulated by bush elements, which connect the beam elements involved along the overlap. To simulate the 1D-bar model, the displacements according to the y-axis and the z-axis are fixed. In order for the bush elements to work in shear only, all the stiffnesses are set to unity except that for the shear mode. The latter is computed according to [21]. A preliminary study (not presented in this paper) showed that a number of 100 bush elements regularly distributed along the overlap allows for accurate results at restricted computational time cost. In the adherends, 204 beam elements are set. Moreover, the unbalanced configuration such that $e_2=2e_1=4.8$ mm is under consideration.

4.2.2. PS FE model. The adherends and the adhesive are simulated by quadrangular elements (SAMCEF type T015) under plane stress conditions. The elements chosen have linear interpolation functions and four internal modes. The normal integration scheme is chosen. As the adhesive stresses significantly vary at the overlap edges, the mesh is thus refined in this area through a progressive mesh. The smallest element in the adhesive

layer is then located at both overlap ends and has an aspect ratio equal to 1. A nominal number of four elements in the adhesive layer is chosen (see section 4.2.3), leading to a minimal size of 0.1 mm*0.1 mm. Furthermore, a transition ratio equal to one is set at the interface with the adhesive and a progressive mesh is adopted in the adherends.

4.2.3. 3D FE model. The adherends and the adhesive are simulated by 3D brick elements (SAMCEF type T008). The elements chosen have linear interpolation functions and 9 internal modes (8 nodes and 24 degrees of freedom). The normal integration scheme is chosen. The mesh of the 3D-model consists in an extrusion in the width direction of the PS FE model mesh. Symmetry conditions are applied in an external plane, the normal of which is the direction of extrusion. The stresses are measured along the middle line of the adhesive layer and on the symmetry plane.

The maximum value of adhesive shear and peeling stresses depends on the mesh density. As the objective of this comparison of PS and 3D FE predictions is to assess the relevance of the 1D-beam model, the dependency of shear and peeling peaks on the mesh density has to be addressed. The study consists then in measuring the maximum values of the adhesive shear and peeling stresses as a function of the number of elements in the adhesive layer thickness. The number of elements in the adhesive layer varies, while keeping the aspect ratio of the smallest element in the adhesive layer (located at both overlap ends) equal to 1. It is shown that the shear (peeling) peak increases (decreases) with the increasing number of elements in the adhesive layer (see Fig. 13). However, this increasing or decreasing tendency significantly slows down with the increasing number of elements. Tab. 2 shows changes to the adhesive shear and peeling peaks for varying numbers of elements, relative to those for 32 elements. It can be observed that these relative differences are quite low, except for the peeling peak for the case with 2 elements. It could be thought that the hypothesis of an elastic perfectly plastic adhesive material behavior allows for the saturation of the adhesive peak stresses, contributing to low variations. In order to understand the elevated difference on the peak stress for the case with 2 elements, the shear and peeling peak adhesive stress

on the upper (or lower) external line of the adhesive layer is measured while the number of elements varies. These peaks on the adhesive upper (or lower) line are located at overlap ends, as for the adhesive middle line. As shown in Fig. 14, whereas the increase of the number of elements in the adhesive layer decreases the relative difference to the middle line on the shear peak, this relative difference increases significantly. The influence of the edge effect on the adhesive stress at the middle line seems thus to be reduced by refining the mesh in the adhesive thickness. Finally, it is considered that almost steady values for shear and adhesive peaks can be obtained, when the side height of the smallest element in the adhesive layer is inferior to 0.1 mm (i.e.: four elements in an adhesive thickness of 0.4 mm).

4.3. Comparison of results

4.3.1. 1D-bar present model vs. 1D-bar FE model. Firstly, it is indicated (not presented here) that, when the adhesive is supposed linear elastic, the 1D-bar present model (without any shear in the adherends) and 1D-bar FE model provide exactly the same adhesive shear stress distribution along the overlap. Considering the elasto-plastic behavior of the adhesive, the 1D-bar present model (without any shear in the adherends) and 1D-bar FE model provide exactly the same adhesive shear stress distribution along the overlap, for the balanced and unbalanced configuration, as shown in Fig. 15 and Fig. 16, respectively.

4.3.2. 1D-beam present model vs. PS and 3D FE models. The 1D-beam present model with a linear shear stress in the adherends is compared to the PS and 3D FE models, in case of a balanced configuration for example. The distribution of the adhesive shear, peeling and Von Mises stresses along the overlap are provided in Fig. 17, Fig. 18 and Fig. 19. Although the stress tensor component number is restricted to two in the 1D-beam present model, a good agreement is shown.

4.3.3. *Evolution of adhesive stress distribution with the applied load.* In order to illustrate the effect of plasticity of the adhesive stress distribution, the adhesive shear, peeling and Von Mises stress distribution obtained with the 1D-beam present model are provided in Fig. 20, Fig. 21 and Fig. 22 respectively, at two intermediate applied loads (5 N.mm⁻¹ and 7 N.mm⁻¹). The structure chosen is the unbalanced configuration such that $e_2=2e_1=4.8$ mm. The adhesive layer is meshed with four elements in its thickness (leading to a side length of 0.1 mm for the smallest element). Furthermore, the stress distributions at an applied load of 10 N.mm⁻¹ are compared to those predicted by the 3D FE models, resulting in a good agreement. Moreover, it appears that the adhesive stress peak saturation is balanced by the increase of the minimal adhesive stress level reached along the overlap.

4.4. *Assessment of the relevance of the model*

In order to assess the relevance of the present 1D-beam model, unbalanced configurations such that $e_2=2e_1=4.8$ mm with isotropic adherends are under consideration. The study described in this section consists of measuring the relative differences between the 3D FE model predictions and the 1D-beam model predictions, in terms of adhesive shear and peeling stresses, when: (i) the adherend stiffness varies, (ii) the adhesive thickness varies. Concerning the influence of the adherend stiffness, the variation of the adherend stiffness is achieved by fixing the Young's modulus of the adherend 1 at its value in Tab. 1 ($E_1=72$ GPa), while the Young's modulus of the adherend 2 is varying such $E_2=(0.5, 1, 2, 3)*E_1$. In the 3D FE model, the adhesive layer is meshed with four elements in its thickness (leading to a side length of 0.1 mm for the smallest element). As shown in Tab. 3, the 1D-beam model provides adhesive shear and peeling peaks very closed to those predicted by the 3D FE model, with relative differences inferior to 10%. Moreover, in term of stress distribution along the overlap, a good correlation is obtained, as shown in Fig. 23 to Fig. 25 for the case $E_2/E_1=3$. In particular, the overstress for abscissas close to zero, due to the unbalance of the joint, is correctly retrieved. Concerning the influence of the adhesive thickness, five adhesive

layer thicknesses are chosen: 0.1 mm, 0.2 mm, 0.3 mm, 0.4 mm and 0.5 mm. In the 3D FE model, the number of elements in the adhesive thickness is taken such that the side length of the smallest element is equal to 0.5 mm (e.g.: 8 elements in an adhesive thickness of 0.4mm). As shown in Tab. 4, the 1D-beam model provides adhesive shear and peeling peaks very close to the ones predicted by the 3D FE model (see Fig. 20 to Fig. 22, for the case $e=0.4$ mm), with relative differences inferior to 10%, except for the peeling peak for an adhesive thickness of 0.1 mm. However, when the adhesive thickness is equal to 0.1 mm, it is meshed with only 2 elements, resulting in a significant influence of edge effects on the peeling stress at overlap ends when measured in the adhesive middle line (see section 4.2.3).

Finally, the computation times required for the FE models of section 4.2.3, when the number of elements in the adhesive thickness varies, are expressed as functions of the computation time recorded for the 1D-beam model (equal to 1.3 s). All the computations are performed on the same computer (HP Z800). Tab. 5 shows that the less refined mesh is consuming 49 times more of computation time than the 1D-beam model. Nevertheless, it is underlined that the 3D FE models allows for a more refined stress analysis than the simplified approaches.

5. CONCLUSION

A 1D-bar and 1D-beam simplified approach for the stress analysis of bonded joints involving an elasto-plastic adhesive is presented and illustrated for the single-lap joint configuration. The example of the single-lap bonded joint configuration should not be seen as a restriction, since various single-lap geometries could be simulated through simple manipulations of the structure stiffness matrix. The simplified approach, relying on the simplifying hypotheses provided in section 2.1.1.1 and section 2.2.1.1, is based on the formulation of a 4-node macro-element able to simulate a full bonded overlap. Firstly, 1D-bar and 1D-beam macro-elements are formulated assuming a linear elastic adhesive behavior and taking into account a linear variation of the shear stress in the

adherends. It is shown that the same hypotheses lead to the same results when the adhesive stress distributions along the overlap are compared with the reference ones. Secondly, an iterative procedure, employing the linear elastic computation of the stiffness matrix, is presented to take into account an elasto-plastic adhesive behavior. Assuming a yield function (elastic perfectly plastic behavior) and a yield criterion, the residue vector is computed through the projection of the current stress state, up to reaching equilibrium for a prescribed tolerance. Finally, the results provided by the models based on the simplified approach are compared to those of 1D-bar, PS and 3D FE models, assuming an elastic perfectly plastic adhesive behavior. A good agreement is shown.

ACKNOWLEDGMENT

The three first authors gratefully acknowledge for their support the SOGETI HIGH TECH engineers and managers, involved in the development of JoSAT (Joint Stress Analysis Tool) internal research program.

REFERENCES

1. J.W. van Ingen, A. Vlot, Stress Analysis of Adhesively Bonded Single Lap Joints, Report LR-470, Delft University of Technology, April 1993.
2. M.Y. Tsai, J. Morton, Int. J. Solids Structures, Vol. 31, No. 18, pp. 2537-2563 (1994).
3. L.F.M. da Silva, P.J.C das Neves, R.D. Adams, J.K. Spelt, Int. J. Adhesion and Adhesives, Vol. 29, pp. 319-330 (2009).
4. L.J. Hart-Smith, Technical Report, NASA, CR112236 (1973).

5. D.A. Bigwood, A.D. Crocombe, *Int. J. Adhesion and Adhesives*, Vol. 10, No. 1, pp. 31-41 (1990).
6. R.D. Adams, V. Mallick, *J. Adhesion*, Vol. 38, pp. 199-217 (1992).
7. L. Tong, M. Kuruppu, D. Kelly, *J. Thermoplastics Composite Materials*, Vol. 10, pp. 61-75 (1997).
8. F. Mortensen, *Development of Tools for Engineering Analysis and Design of High-Performance FRP-Composite Structural Elements*, PhD Dissertation, Aalborg University, Sweden (1998).
9. S.S. Smeltzer III, *An Inelastic Methodology for Bonded Joints with Shear Deformable, Anisotropic Adherends*, PhD Thesis, North Carolina State University, Raleigh, NC (2003).
10. E. Oterkus, A. Barut, E. Madenci, S.S. Smeltzer III, D.R. Ambur, 45th AIAA/ASME/ASCE/AHS/ASC Structures, Structural Dynamics & Materials Conference, 19-22 April 2004, Palm Springs, California
11. C. Yang, H. Huang, J.S. Tomblin, W. Sun, *J. Composite Materials*, Vol. 38, No. 4, pp. 293-309 (2004).
12. E. Paroissien, M. Sartor, J. Huet, in: *Advanced in Integrated Design and Manufacturing in Mechanical Engineering II*, Springer Eds., Part 3, pp. 95-110 (2007).
13. E. Paroissien, M. Sartor, J. Huet, F. Lachaud, *AIAA J. Aircraft*, Vol. 44, No. 2, pp. 573-582 (2007).

14. S.E. Stapleton, The Analysis of Adhesively Bonded Advanced Composite Joints using Joint Finite Elements, PhD Dissertation, University of Michigan, USA (2012).
15. E. Paroissien, A. Da Veiga, A. Laborde, in: *Proceedings of the 26th Symposium of the International Committee on Aeronautical Fatigue*, Montreal, pp. 359-374 (2011).
16. M.Y. Tsai, D.W. Oplinger, J. Morton, *Int. J. Solids Structure*, Vol.35, No.12, pp. 1163-1185 (1998).
17. M. Goland and E. Reissner, *J. Appl. Mech.*, Vol. 11, pp. A17-27 (1944).
18. J.L. Högberg, Mechanical Behavior of Single-Layer Adhesive Joints – An Integrated Approach, MsC Thesis, Department of Applied Mechanics, Chalmers University of Technology, SW (2004).
19. J. Lubliner, *Plasticity theory*, Macmillan, New York (1990).
20. J.Y. Cognard, R. Créac’hcadec, L. Sohier, D. Leguillon, *Int. Journal of Adhesives and Adhesion*, 30, No. 5, pp. 257-266 (2010).
21. C. Dechwayukul, C.A. Rubin, and G.T. Hahn, *AIAA J. Aircraft*, Vol. 41, No.11, pp.2216-2228 (2003).

APPENDIX A

This appendix details the resolution of the differential in equation (24). The characteristic polynomial expression is:

$$\begin{cases} P(R) = \hat{a}R^3 + \hat{b}R^2 + \hat{c}R + \hat{d} = 0 \\ R = r^2 \\ \hat{a} = 1 \\ \hat{b} = -k_1 \\ \hat{c} = k_4 \\ \hat{d} = k_2k_3 - k_1k_4 \end{cases}$$

(A.1)

To determine these roots, the Cardan's method is employed. Then, equation (A.1) is modified as:

$$\begin{cases} R'^3 + \hat{p}R' + \hat{q} = 0 \\ \hat{p} = -\frac{k_1^2}{3} + k_4 \\ \hat{q} = -\frac{k_1}{27}(2k_1^2 - 9k_4) + k_2k_3 - k_1k_4 \end{cases} \quad (\text{A.2})$$

where:

$$R' = R - \frac{k_1}{3} \quad (\text{A.3})$$

and the determinant is:

$$\hat{\Delta} = \hat{q}^2 + \frac{4}{27}\hat{p}^3 \quad (\text{A.4})$$

By defining:

$$\begin{cases} \hat{u} = \sqrt[3]{\frac{-\hat{q} + \sqrt{\hat{\Delta}}}{2}} \\ \hat{v} = \sqrt[3]{\frac{-\hat{q} - \sqrt{\hat{\Delta}}}{2}} \end{cases} \quad (\text{A.5})$$

The roots of the reduced equation are written as:

$$\begin{cases} R'_1 = \hat{u} + \hat{v} \\ R'_2 = j\hat{u} + j\bar{\hat{v}} \\ R'_3 = j^2\hat{u} + j^2\bar{\hat{v}} \end{cases} \quad (\text{A.6})$$

Consequently, the roots of the characteristic equation (A.1) are given by:

$$\begin{cases} R_1 = \hat{u} + \hat{v} + \frac{k_1}{3} = r^2 \\ R_2 = -\frac{1}{2}(\hat{u} + \hat{v}) + \frac{k_1}{3} + i\frac{\sqrt{3}}{2}(\hat{u} - \hat{v}) = (s + it)^2 \\ R_3 = -\frac{1}{2}(\hat{u} + \hat{v}) + \frac{k_1}{3} - i\frac{\sqrt{3}}{2}(\hat{u} - \hat{v}) = (s - it)^2 \end{cases} \quad (\text{A.7})$$

Finally, the adhesive stresses have to be determined as:

$$\begin{cases} S(x) = \begin{bmatrix} \overline{K_1}e^{sx} \sin(tx) + \overline{K_2}e^{sx} \cos(tx) + \overline{K_3}e^{-sx} \sin(tx) \\ + \overline{K_4}e^{-sx} \cos(tx) + \overline{K_5}e^{rx} + \overline{K_6}e^{-rx} \end{bmatrix} \\ T(x) = \begin{bmatrix} K_1e^{sx} \sin(tx) + K_2e^{sx} \cos(tx) + K_3e^{-sx} \sin(tx) \\ + K_4e^{-sx} \cos(tx) + K_5e^{rx} + K_6e^{-rx} + K_7 \end{bmatrix} \\ r = \sqrt{\hat{u} + \hat{v} + \frac{k_1}{3}} \\ s = \sqrt{\frac{1}{2}(\text{Re}(R_2) + |R_2|)} \\ t = \sqrt{\frac{1}{2}(|R_2| - \text{Re}(R_2))} \end{cases} \quad (\text{A.8})$$

APPENDIX B

Determination of nodal displacements and forces.

With the equations (18) and (19), it is possible to express the derivatives of the longitudinal and transverse displacements as a function of the adhesive stresses and its derivatives:

$$\left\{ \begin{array}{l} \frac{d^4 w_1}{dx^4} = A_{10} \frac{dT}{dx} + B_{10} S \\ \frac{d^4 w_2}{dx^4} = A_{20} \frac{dT}{dx} + B_{20} S \\ \frac{d^3 u_1}{dx^3} = C_{10} \frac{dT}{dx} + D_{10} S \\ \frac{d^3 u_2}{dx^3} = C_{20} \frac{dT}{dx} + D_{20} S \end{array} \right. \quad (\text{B.1})$$

where:

$$\left\{ \begin{array}{l} A_{10} = -\frac{b}{2\Delta_1} [2B_1 + e_1 A_1] \quad ; \quad B_{10} = -\frac{A_1 b}{\Delta_1} \\ A_{20} = \frac{b}{2\Delta_2} [2B_2 - e_2 A_2] \quad ; \quad B_{20} = \frac{A_2 b}{\Delta_2} \\ C_{10} = -\frac{b}{2\Delta_1} [e_1 B_1 + 2D_1] \quad ; \quad D_{10} = -\frac{B_1 b}{\Delta_1} \\ C_{20} = \frac{b}{2\Delta_2} [-e_2 B_2 + 2D_2] \quad ; \quad D_{20} = \frac{B_2 b}{\Delta_2} \end{array} \right. \quad (\text{B.2})$$

To obtain the expressions of displacements in the adherends, equations (B.1) have to be integrated. Before integrating equation (B.1), the differential equations (19) are written as:

$$\begin{cases} S = \frac{1}{k_2k_3 - k_1k_4} \left[k_3 \frac{d^3T}{dx^3} + k_1 \frac{d^4S}{dx^4} \right] \\ \frac{dT}{dx} = \frac{1}{k_1k_4 - k_2k_3} \left[k_4 \frac{d^3T}{dx^3} + k_2 \frac{d^4S}{dx^4} \right] \end{cases} \quad (\text{B.3})$$

and introduced in equations (B.1) The displacements in the adherends are then expressed as:

(B.4)

$$\begin{cases} w_1 = \left[\frac{A_{10}k_4 - B_{10}k_3}{(k_1k_4 - k_2k_3)^2} \left(k_4 \frac{dT}{dx} + k_2 \frac{d^2S}{dx^2} \right) + \frac{A_{10}k_2 - B_{10}k_1}{k_1k_4 - k_2k_3} S + J_0 \left(\frac{x}{\Delta} \right)^3 + J_1 \left(\frac{x}{\Delta} \right)^2 + J_2 \frac{x}{\Delta} + J_3 \right] \\ w_2 = \left[\frac{A_{20}k_4 - B_{20}k_3}{(k_1k_4 - k_2k_3)^2} \left(k_4 \frac{dT}{dx} + k_2 \frac{d^2S}{dx^2} \right) + \frac{A_{20}k_2 - B_{20}k_1}{k_1k_4 - k_2k_3} S + \bar{J}_0 \left(\frac{x}{\Delta} \right)^3 + \bar{J}_1 \left(\frac{x}{\Delta} \right)^2 + \bar{J}_2 \frac{x}{\Delta} + \bar{J}_3 \right] \\ u_1 = \left[\frac{C_{10}k_4 - D_{10}k_3}{k_1k_4 - k_2k_3} T + \frac{C_{10}k_2 - D_{10}k_1}{k_1k_4 - k_2k_3} \frac{dS}{dx} + J_4 \left(\frac{x}{\Delta} \right)^2 + J_5 \frac{x}{\Delta} + J_6 \right] \\ u_2 = \left[\frac{C_{20}k_4 - D_{20}k_3}{k_1k_4 - k_2k_3} T + \frac{C_{20}k_2 - D_{20}k_1}{k_1k_4 - k_2k_3} \frac{dS}{dx} + \bar{J}_4 \left(\frac{x}{\Delta} \right)^2 + \bar{J}_5 \frac{x}{\Delta} + \bar{J}_6 \right] \\ \theta_1 = \left[\frac{A_{10}k_4 - B_{10}k_3}{k_1k_4 - k_2k_3} (T - K_7) + \frac{A_{10}k_2 - B_{10}k_1}{k_1k_4 - k_2k_3} \frac{dS}{dx} + 3J_0 \frac{x^2}{\Delta^3} + 2J_1 \frac{x}{\Delta^2} + \frac{J_2}{\Delta} \right] \\ \theta_2 = \left[\frac{A_{20}k_4 - B_{20}k_3}{k_1k_4 - k_2k_3} (T - K_7) + \frac{A_{20}k_2 - B_{20}k_1}{k_1k_4 - k_2k_3} \frac{dS}{dx} + 3\bar{J}_0 \frac{x^2}{\Delta^3} + 2\bar{J}_1 \frac{x}{\Delta^2} + \frac{\bar{J}_2}{\Delta} \right] \end{cases}$$

Fourteen new integration constants are involved. However, following the resolution scheme in [18], the total number of integration constants can be reduced to twelve.

Firstly, the second equation of system (18) gives:

$$\frac{dN_2}{bdx} = T \Rightarrow A_2 \frac{d^2u_2}{dx^2} - B_2 \frac{d^3w_2}{dx^3} = bT \quad (\text{B.5})$$

Hence:

$$A_2 \frac{2\bar{J}_4}{\Delta^2} - B_2 \frac{6\bar{J}_0}{\Delta^3} = bK_7 \Rightarrow \bar{J}_4 = \frac{b\Delta^2 K_7}{2A_2} + \frac{3B_2 \bar{J}_0}{A_2 \Delta} \quad (\text{B.6})$$

In the same way, by considering the adherend 2, it becomes:

$$J_4 = -\frac{b\Delta^2 K_7}{2A_1} + \frac{3B_1 J_0}{A_1 \Delta} \quad (\text{B.7})$$

Secondly, the difference between the transverse displacements of both adherends provides:

$$w_1 - w_2 = \frac{e}{E} S + (J_0 - \bar{J}_0) \left(\frac{x}{\Delta} \right)^3 + (J_1 - \bar{J}_1) \left(\frac{x}{\Delta} \right)^2 + (J_2 - \bar{J}_2) \frac{x}{\Delta} + J_3 - \bar{J}_3 \quad (\text{B.8})$$

According to the definition of the peeling stress, it becomes:

$$\bar{J}_i = J_i ; i = 1,3 \quad (\text{B.9})$$

The difference of the longitudinal displacement provides:

$$u_2 - u_1 - \frac{1}{2} e_1 \theta_1 - \frac{1}{2} e_2 \theta_2 = \frac{e}{G} T + P(x) \quad (\text{B.10})$$

where $P(x)$ is a quadratic polynomial, all coefficients of which have to be equal to zero:

$$\bar{J}_4 - J_4 - \frac{3}{2} e_1 \frac{J_0}{\Delta} - \frac{3}{2} e_2 \frac{\bar{J}_0}{\Delta} = 0 \quad (\text{B.11})$$

$$\bar{J}_5 - J_5 - e_1 \frac{J_1}{\Delta} - e_2 \frac{\bar{J}_1}{\Delta} = 0 \quad (\text{B.12})$$

$$\bar{J}_6 - J_6 - \frac{e_1}{2} \frac{J_2}{\Delta} - \frac{e_2}{2} \frac{\bar{J}_2}{\Delta} + \frac{K_7}{k_1 k_4 - k_2 k_3} \left[\begin{array}{c} k_4 \left(\frac{e_1}{2} A_{10} + \frac{e_2}{2} A_{20} \right) \\ - k_3 \left(\frac{e_1}{2} B_{10} + \frac{e_2}{2} B_{20} \right) \end{array} \right] = 0 \quad (\text{B.13})$$

The displacements in the adherends are then expressed under the shape of equations (27), with:

$$\left\{ \begin{array}{l} \tilde{\beta}_1 = \frac{C_{10} k_4 - D_{10} k_3}{k_1 k_4 - k_2 k_3} \quad ; \quad \bar{\beta}_1 = \frac{C_{10} k_2 - D_{10} k_1}{k_1 k_4 - k_2 k_3} \\ \tilde{\beta}_2 = \frac{C_{20} k_4 - D_{20} k_3}{k_1 k_4 - k_2 k_3} \quad ; \quad \bar{\beta}_2 = \frac{C_{20} k_2 - D_{20} k_1}{k_1 k_4 - k_2 k_3} \\ \tilde{\beta}_5 = \frac{A_{10} k_4 - B_{10} k_3}{k_1 k_4 - k_2 k_3} \quad ; \quad \bar{\beta}_5 = \frac{A_{10} k_2 - B_{10} k_1}{k_1 k_4 - k_2 k_3} \\ \tilde{\beta}_6 = \frac{A_{20} k_4 - B_{20} k_3}{k_1 k_4 - k_2 k_3} \quad ; \quad \bar{\beta}_6 = \frac{A_{20} k_2 - B_{20} k_1}{k_1 k_4 - k_2 k_3} \\ \tilde{\beta}_3 = \frac{\tilde{\beta}_5}{k_1 k_4 - k_2 k_3} \quad ; \quad \tilde{\beta}_4 = \frac{\tilde{\beta}_6}{k_1 k_4 - k_2 k_3} \\ J_0 = \frac{b \Delta^3 \left(\frac{1}{A_1} + \frac{1}{A_2} \right)}{3(e_1 + e_2) + 6 \left(\frac{B_1}{A_1} - \frac{B_2}{A_2} \right)} K_7 \end{array} \right. \quad (\text{B.14})$$

The constitutive equations (19) allow for the computation of normal and shear forces and of bending moments in both adherends, under the shape of equations (28) with:

$$\left\{ \begin{array}{l} \tilde{a}_1 = A_1 \tilde{\beta}_1 - B_1 \tilde{\beta}_5 \quad ; \quad \bar{a}_1 = A_1 \bar{\beta}_1 - B_1 \bar{\beta}_5 \\ \tilde{a}_2 = A_2 \tilde{\beta}_2 - B_2 \tilde{\beta}_6 \quad ; \quad \bar{a}_2 = A_2 \bar{\beta}_2 - B_2 \bar{\beta}_6 \\ \tilde{a}_3 = -B_1 \tilde{\beta}_1 + D_1 \tilde{\beta}_5 \quad ; \quad \bar{a}_3 = -B_1 \bar{\beta}_1 + D_1 \bar{\beta}_5 \\ \tilde{a}_4 = -B_2 \tilde{\beta}_2 + D_2 \tilde{\beta}_6 \quad ; \quad \bar{a}_4 = -B_2 \bar{\beta}_2 + D_2 \bar{\beta}_6 \end{array} \right. \quad (\text{B.15})$$

APPENDIX C

Modification in the BBe element, induced by a linear shear stress in the adherends.

The equations (21) are modified as:

$$\left\{ \begin{array}{l} \frac{du_1}{dx} = \frac{D_1 N_1 + B_1 M_1 + [D_1 C_1 - B_1 C'_1] \frac{dT}{dx}}{\Delta_1} \\ \frac{d^2 w_1}{dx^2} = \frac{A_1 M_1 + B_1 N_1 + [B_1 C_1 - A_1 C'_1] \frac{dT}{dx}}{\Delta_1} \\ \frac{du_2}{dx} = \frac{D_2 N_2 + B_2 M_2 + [D_2 C_2 - B_2 C'_2] \frac{dT}{dx}}{\Delta_2} \\ \frac{d^2 w_2}{dx^2} = \frac{A_2 M_2 + B_2 N_2 + [B_2 C_2 - A_2 C'_2] \frac{dT}{dx}}{\Delta_2} \end{array} \right. \quad (C.1)$$

The expression of the adhesive shear stress then becomes:

$$\left\{ \begin{array}{l} T = \frac{\tilde{G}}{e} \left(u_2 - u_1 - \frac{1}{2} e_1 \theta_1 - \frac{1}{2} e_2 \theta_2 \right) \\ \tilde{G} = \frac{G}{1 + \xi^2} \\ \xi^2 = \frac{3}{8} \frac{G}{e} \left[\frac{e_1}{G_1} + \frac{e_2}{G_2} \right] \end{array} \right. \quad (C.2)$$

Moreover, the system of differential equations in terms of adhesives stresses (equation 22) becomes:

$$\left\{ \begin{array}{l} \frac{d^3 T}{dx^3} = k'_1 \frac{dT}{dx} + k'_2 S \\ \frac{d^4 S}{dx^4} = -k'_4 S - k'_3 \frac{dT}{dx} \end{array} \right. \quad (C.3)$$

with:

$$\begin{cases}
k'_1 = \frac{k_1}{1 - \alpha_T} \\
k'_2 = \frac{k_2}{1 - \alpha_T} \\
k'_3 = k_3 + k'_1 k_5 \\
k'_4 = k_4 + k'_2 k_5 \\
k_5 = \frac{E}{e} \left[\frac{B_2 C_2 - A_2 C'_2}{\Delta_2} - \frac{B_1 C_1 - A_1 C'_1}{\Delta_1} \right] \\
\alpha_T = \frac{\tilde{G}}{e} \left[\frac{D_1 C_1 - B_1 C'_1}{\Delta_1} - \frac{D_2 C_2 - B_2 C'_2}{\Delta_2} + \frac{e_1}{2} \frac{B_1 C_1 - A_1 C'_1}{\Delta_1} + \frac{e_2}{2} \frac{B_2 C_2 - A_2 C'_2}{\Delta_2} \right]
\end{cases} \quad (C.4)$$

Then, the expressions of constants of equation (B.2) are modified together with the expressions of displacements in equation (27) accordingly:

$$\begin{cases}
A_{10} = -\frac{b}{2\Delta_1} [2B_1 + e_1 A_1] + \frac{B_1 C_1 - A_1 C'_1}{\Delta_1} k'_1 & ; & B_{10} = -\frac{A_1 b}{\Delta_1} + \frac{B_1 C_1 - A_1 C'_1}{\Delta_1} k'_2 \\
A_{20} = \frac{b}{2\Delta_2} [2B_2 - e_2 A_2] + \frac{B_2 C_2 - A_2 C'_2}{\Delta_2} k'_1 & ; & B_{20} = \frac{A_2 b}{\Delta_2} + \frac{B_2 C_2 - A_2 C'_2}{\Delta_2} k'_2 \\
C_{10} = -\frac{b}{2\Delta_1} [e_1 B_1 + 2D_1] + \frac{D_1 C_1 - B_1 C'_1}{\Delta_1} k'_1 & ; & D_{10} = -\frac{B_1 b}{\Delta_1} + \frac{D_1 C_1 - B_1 C'_1}{\Delta_1} k'_2 \\
C_{20} = \frac{b}{2\Delta_2} [-e_2 B_2 + 2D_2] + \frac{D_2 C_2 - B_2 C'_2}{\Delta_2} k'_1 & ; & D_{20} = \frac{B_2 b}{\Delta_2} + \frac{D_2 C_2 - B_2 C'_2}{\Delta_2} k'_2
\end{cases} \quad (C.5)$$

Finally, the last equations to modify are the constants expressing the forces and moments in adherends in equations (B.15):

$$\begin{cases}
\tilde{a}_1 = A_1 \tilde{\beta}_1 - B_1 \tilde{\beta}_5 - C_1 & ; & \bar{a}_1 = A_1 \bar{\beta}_1 - B_1 \bar{\beta}_5 \\
\tilde{a}_2 = A_2 \tilde{\beta}_2 - B_2 \tilde{\beta}_6 - C_2 & ; & \bar{a}_2 = A_2 \bar{\beta}_2 - B_2 \bar{\beta}_6 \\
\tilde{a}_3 = -B_1 \tilde{\beta}_1 + D_1 \tilde{\beta}_5 + C_1 & ; & \bar{a}_3 = -B_1 \bar{\beta}_1 + D_1 \bar{\beta}_5 \\
\tilde{a}_4 = -B_2 \tilde{\beta}_2 + D_2 \tilde{\beta}_6 + C_2 & ; & \bar{a}_4 = -B_2 \bar{\beta}_2 + D_2 \bar{\beta}_6
\end{cases} \quad (C.6)$$

LIST OF FIGURE CAPTIONS

Figure 1. Idealization of a single-lap bonded joint with beam and bonded-beams elements, for example. The dotted lined corresponds to the neutral axis. Geometrical and mechanical parameters.

Figure 2. Free body diagram of elements of the overlap.

Figure 3. Displacements and forces on a BBa element.

Figure 4. Bonded assembly and boundary conditions.

Figure 5. Comparison of the adhesive shear stress distribution along the overlap between the present 1D-bar model with the analysis provided by Tsai and al. [16].

Figure 6. Free body diagrams of infinitesimal adherend elements of the overlap.

Figure 7. Displacements and forces on a BBe element.

Figure 8. Bonded assembly and boundary conditions.

Figure 9. Comparison of the adhesive shear stress distribution along the overlap between the 1D-beam present model and the analysis provided by Tsai and al. [16].

Figure 10. Principle scheme of the resolution algorithm for the elasto-plastic problem.

Figure 11. Numbering of the nodes on the single lap joint meshed.

Figure 12. Plastic zone lengths.

Figure 13. Shear (a.) and peeling (b.) peaks on the adhesive middle line as a function of the number of elements in the adhesive thickness.

Figure 14. Shear (a.) and peeling (b.) peaks on the adhesive upper (or lower) line compared to the shear (a.) and peeling (b.) peak on the adhesive center line, as a function of the number of elements in the adhesive thickness.

Figure 15. Comparison of the adhesive shear stress distribution along the overlap between the 1D-bar present model and 1D-bar FE models, on a balanced structure.

Figure 16. Comparison of the adhesive shear stress distribution along the overlap between the 1D-bar present model and 1D-bar FE models, on an unbalanced structure.

Figure 17. Comparison of the adhesive shear stress distribution along the overlap between the 1D-beam present and PS and 3D FE models, on a balanced structure.

Figure 18. Comparison of the adhesive peeling stress distribution along the overlap between the 1D-beam present model and PS and 3D FE models, on a balanced structure.

Figure 19. Comparison of the adhesive Von Mises stress distribution along the overlap between the 1D-beam present model and PS and 3D FE models, on a balanced structure.

Figure 20. Comparison of the adhesive shear stress distribution along the overlap between the 1D-beam present model and PS and 3D FE models, on an unbalanced structure. The distributions at various intermediated applied forces are shown.

Figure 21. Comparison of the adhesive peeling stress distribution along the overlap between the 1D-beam present model and PS and 3D FE models, on an unbalanced structure. The distributions at various intermediated applied forces are shown.

Figure 22. Comparison of the adhesive Von Mises stress distribution along the overlap between the 1D-beam present model and PS and 3D FE models, on an unbalanced structure. The distributions at various intermediated applied forces are shown.

Figure 23. Comparison of the adhesive shear stress distribution along the overlap between the 1D-beam present model and 3D FE models, on an unbalanced structure.

Figure 24. Comparison of the adhesive peeling stress distribution along the overlap between the 1D-beam present model and 3D FE models, on an unbalanced structure.

Figure 25. Comparison of the adhesive Von Mises stress distribution along the overlap between the 1D-beam present model and 3D FE models, on an unbalanced structure.

FIGURES

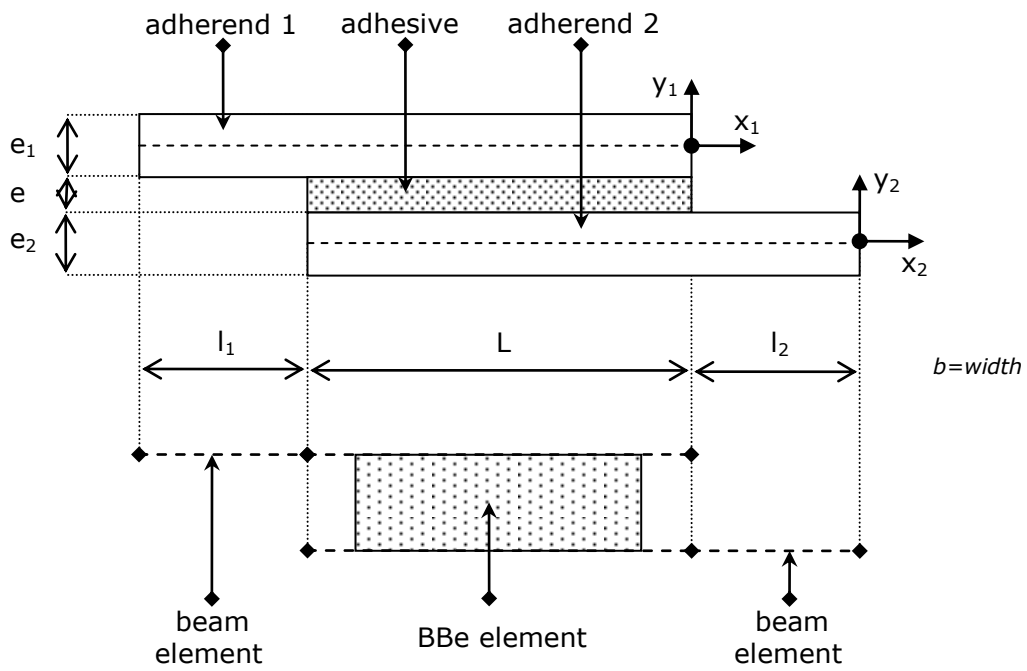


Figure 1. Idealization of a single-lap bonded joint with beam and bonded-beams elements, for example. The dotted lined corresponds to the neutral axis. Geometrical and mechanical parameters.

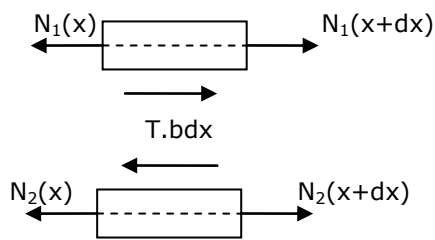


Figure 2. Free body diagram of elements of the overlap.

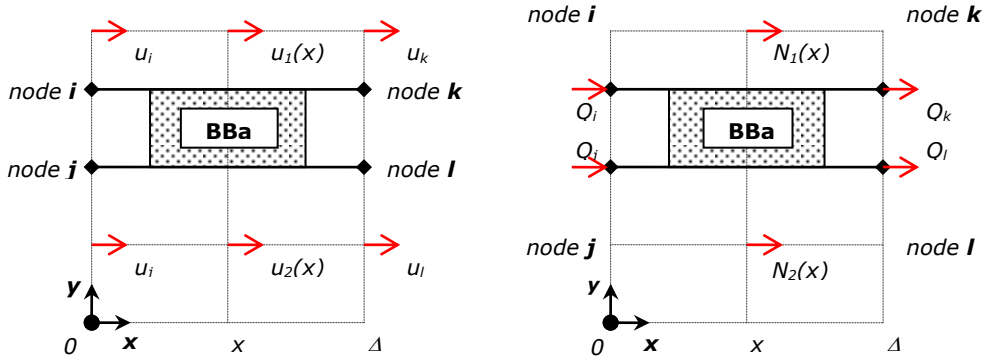


Figure 3. Displacements and forces on a BBa element.

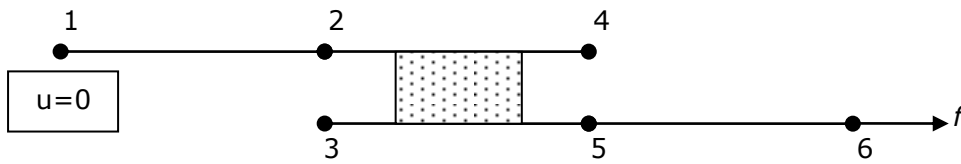


Figure 4. Bonded assembly and boundary conditions.

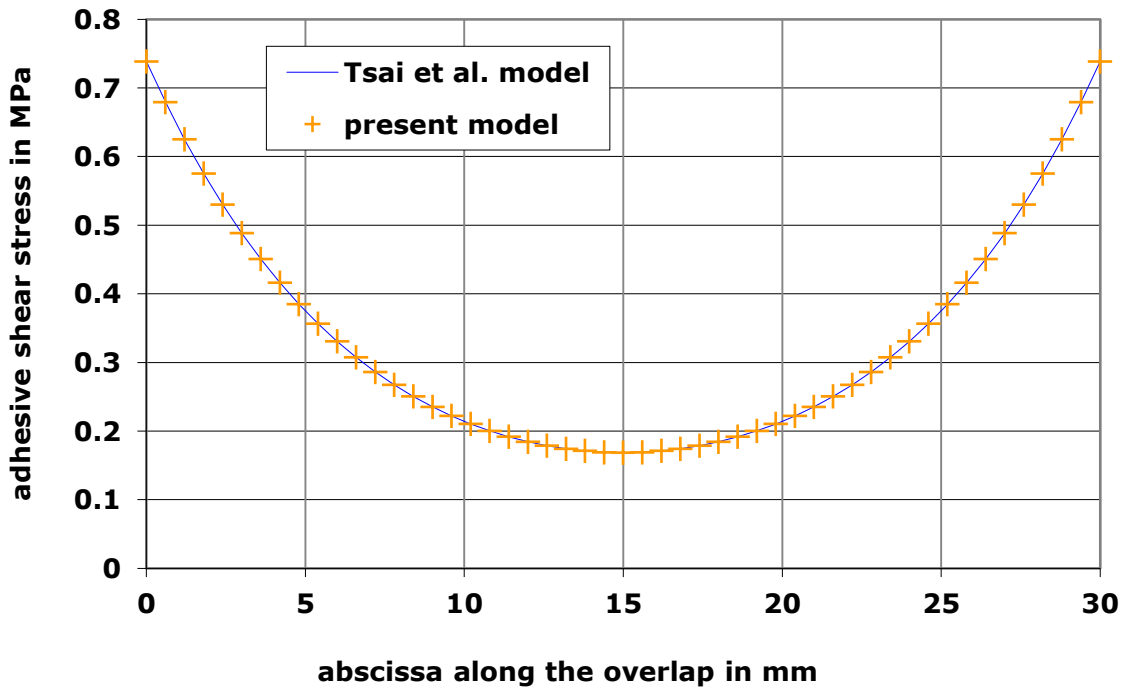


Figure 5. Comparison of the adhesive shear stress distribution along the overlap between the present 1D-bar model with the analysis provided by Tsai and al. [16].

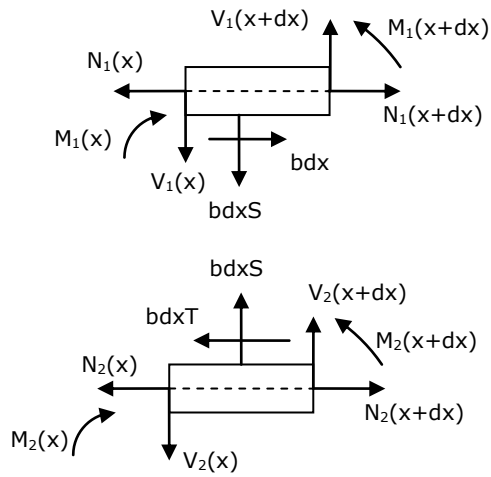


Figure 6. Free body diagrams of infinitesimal adherend elements of the overlap.

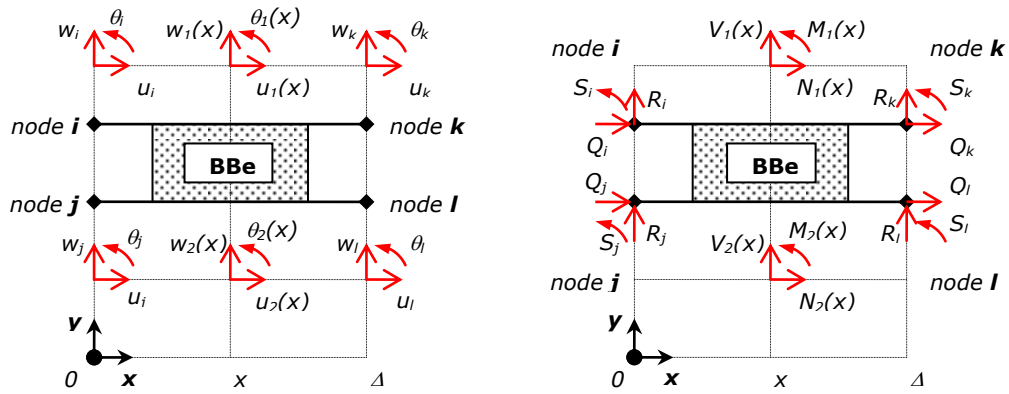


Figure 7. Displacements and forces on a BBe element.

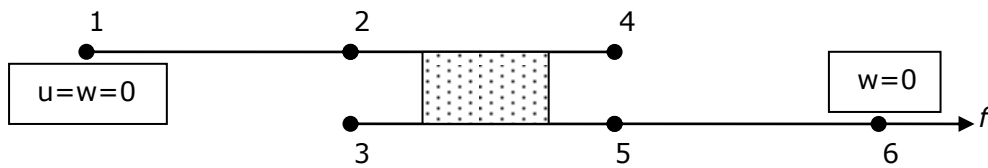


Figure 8. Bonded assembly and boundary conditions.

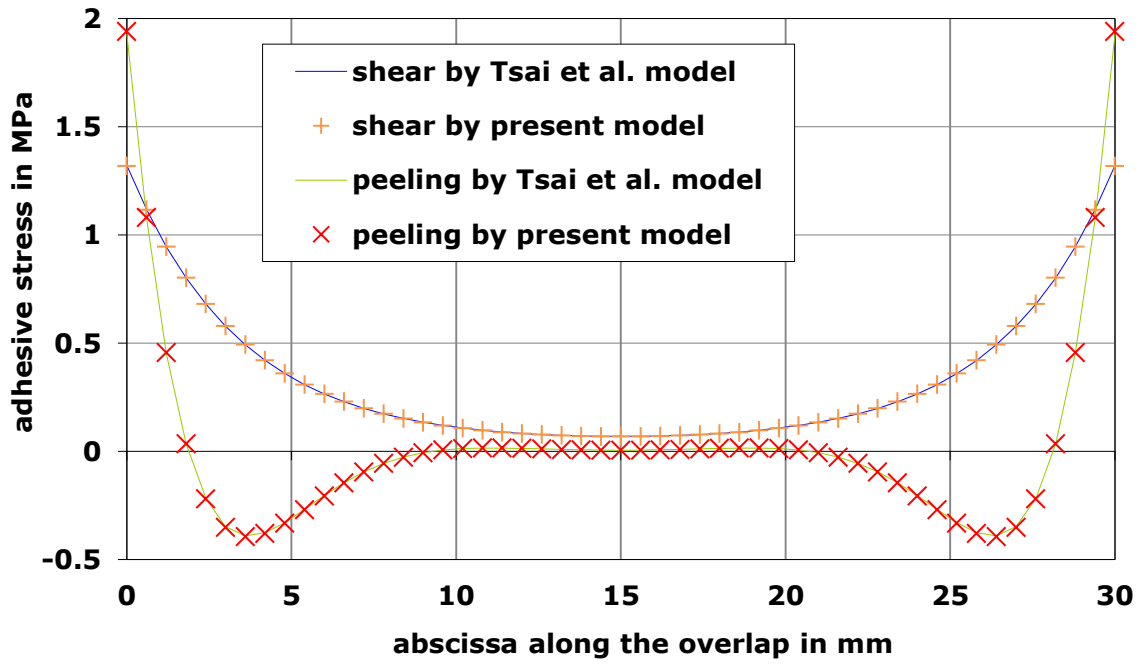


Figure 9. Comparison of the adhesive shear stress distribution along the overlap between the 1D-beam present model and the analysis provided by Tsai and al. [16].

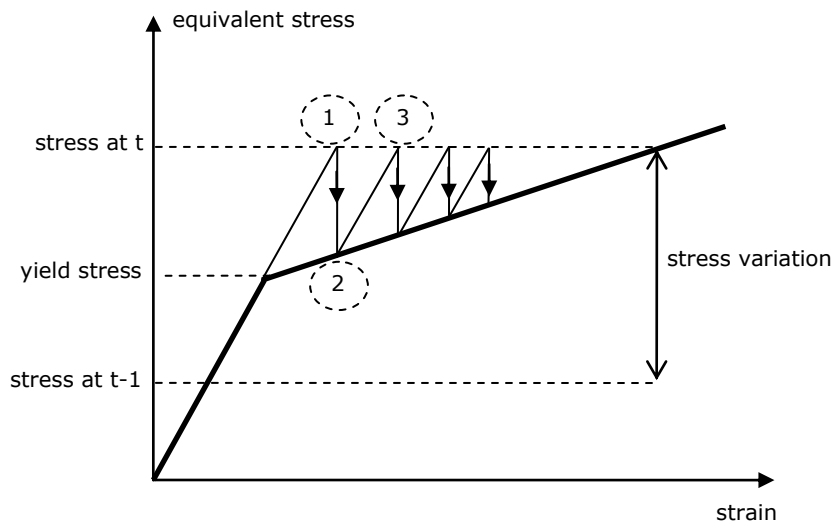


Figure 10. Principle scheme of the resolution algorithm for the elasto-plastic problem.

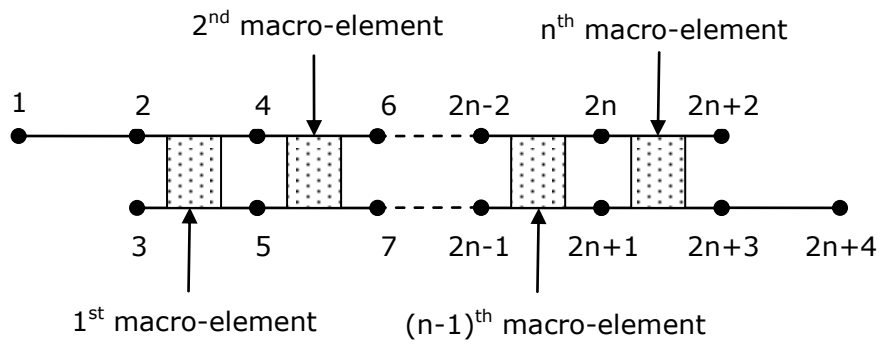


Figure 11. Numbering of the nodes on the single lap joint meshed.

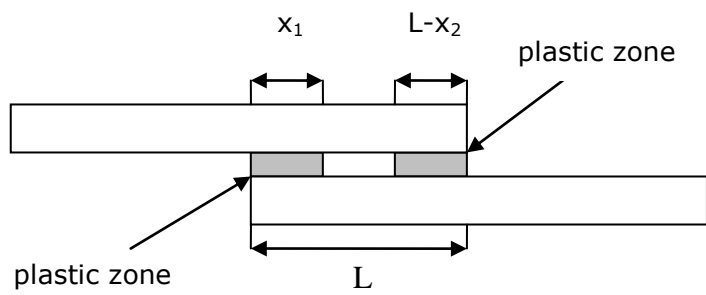
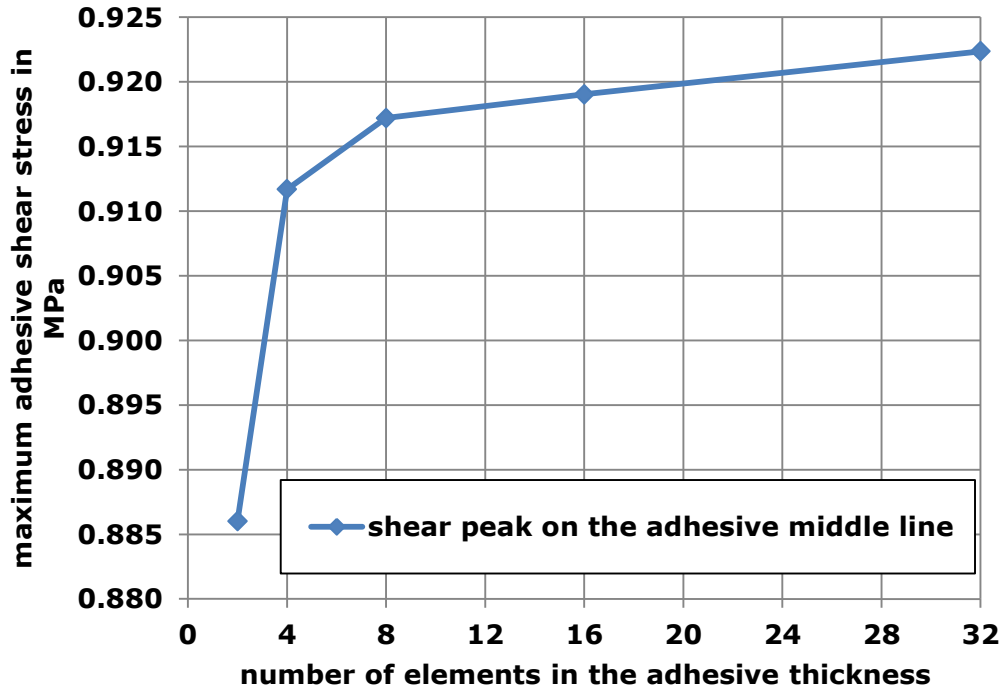
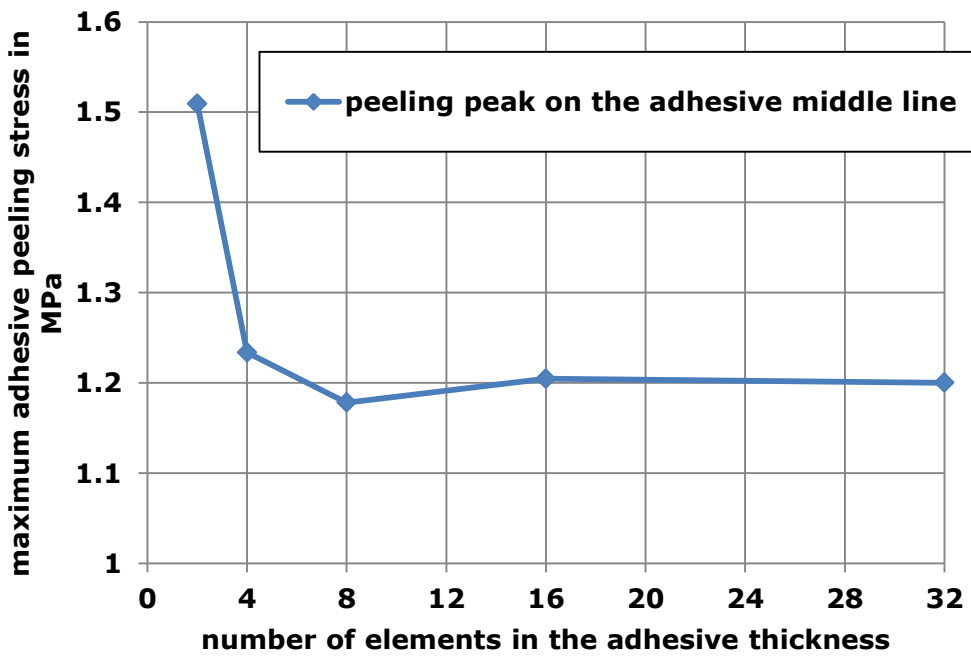


Figure 12. Plastic zone lengths.

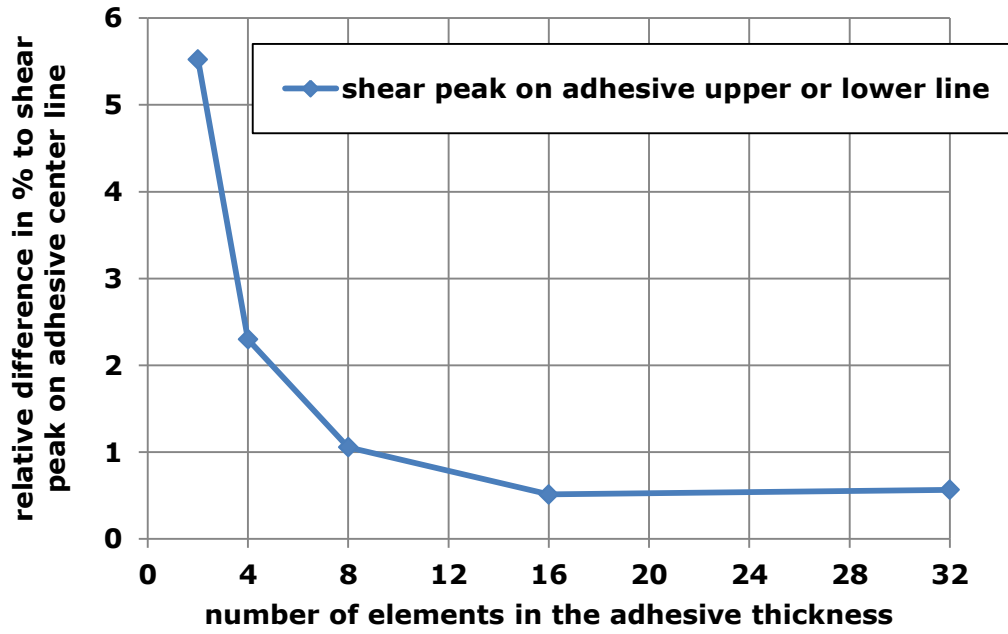


a.

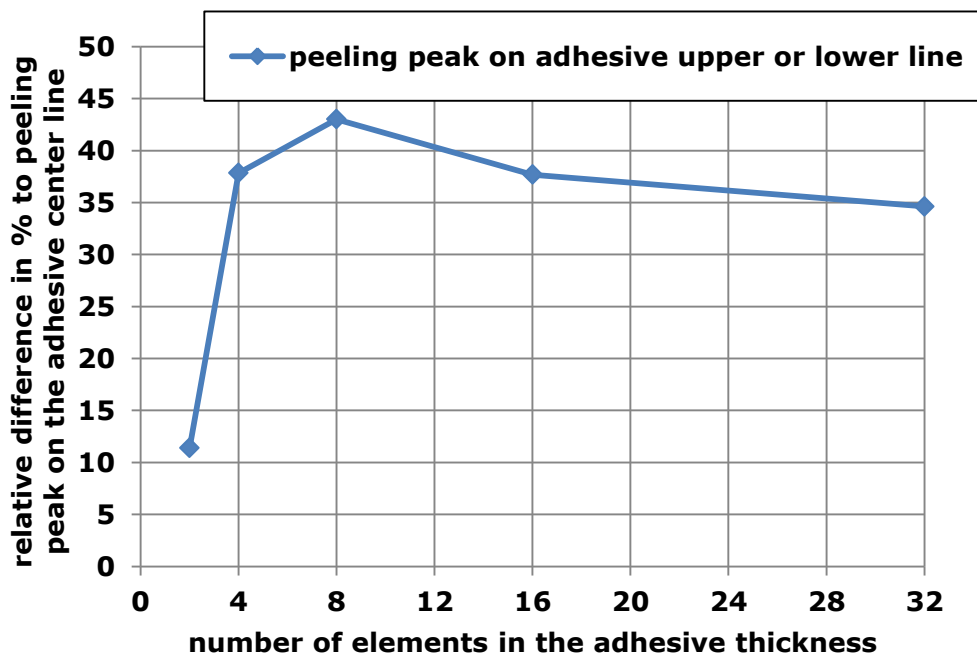


b.

Figure 13. Shear (a.) and peeling (b.) peaks on the adhesive middle line as a function of the number of elements in the adhesive thickness.



a.



b.

Figure 14. Shear (a.) and peeling (b.) peaks on the adhesive upper (or lower) line compared to the shear (a.) and peeling (b.) peak on the adhesive center line, as a function of the number of elements in the adhesive thickness.

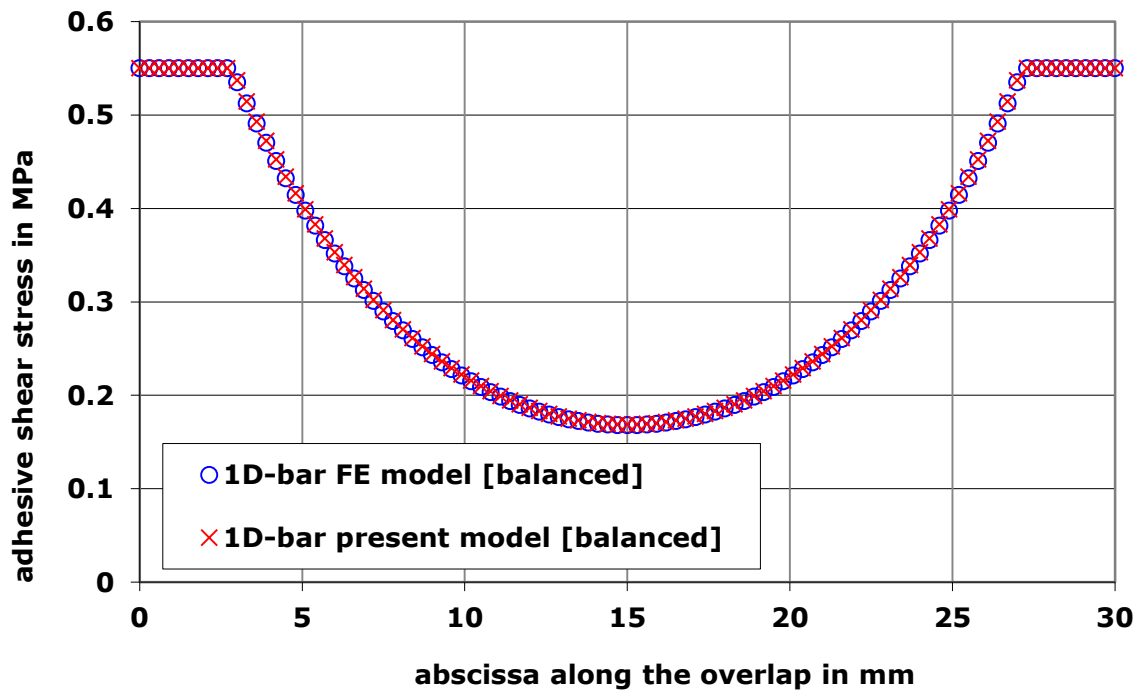


Figure 15. Comparison of the adhesive shear stress distribution along the overlap between the 1D-bar present model and 1D-bar FE models, on an balanced structure.

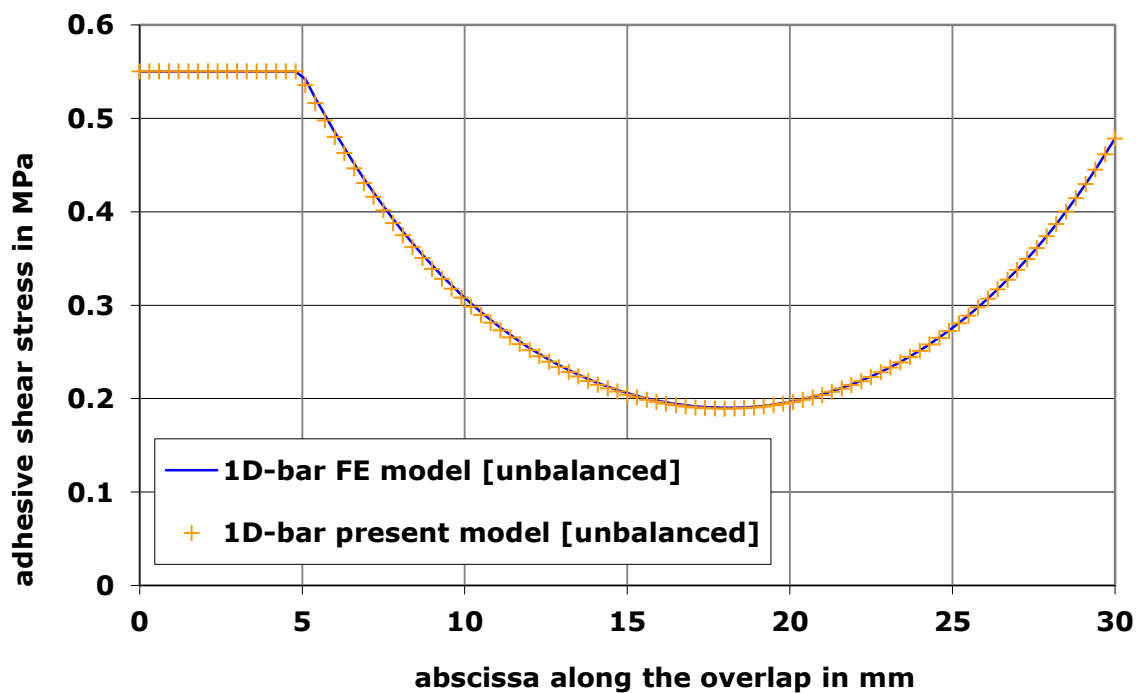


Figure 16. Comparison of the adhesive shear stress distribution along the overlap between the 1D-bar present model and 1D-bar FE models, on an unbalanced structure.

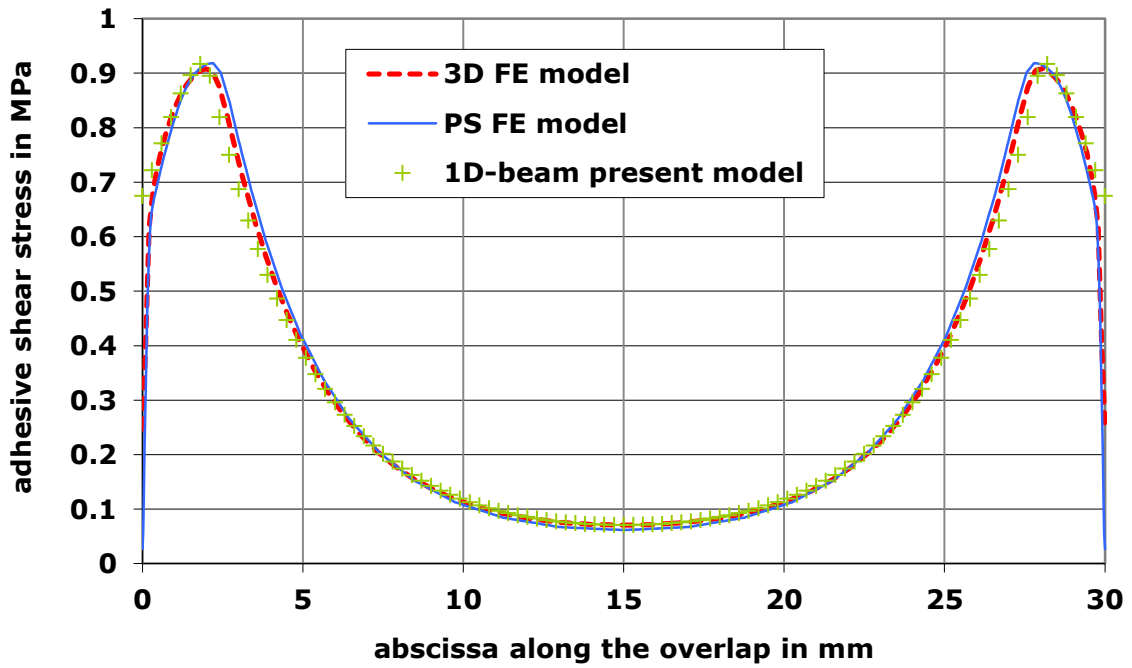


Figure 17. Comparison of the adhesive shear stress distribution along the overlap between the 1D-beam present and PS and 3D FE models, on a balanced structure.

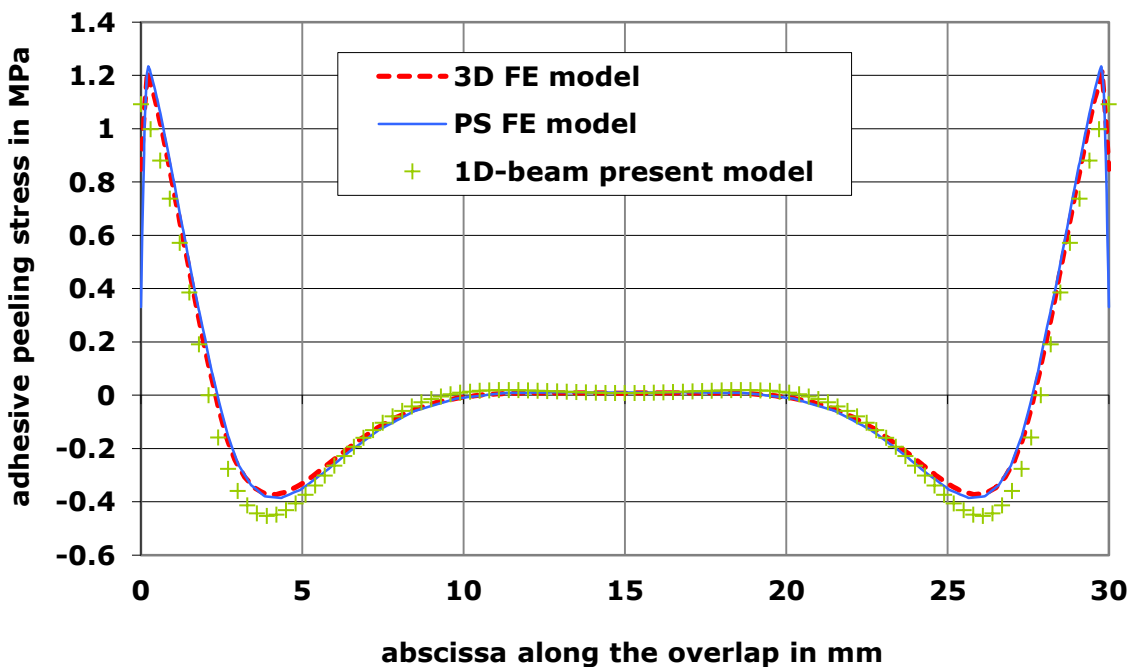


Figure 18. Comparison of the adhesive peeling stress distribution along the overlap between the 1D-beam present model and PS and 3D FE models, on a balanced structure.

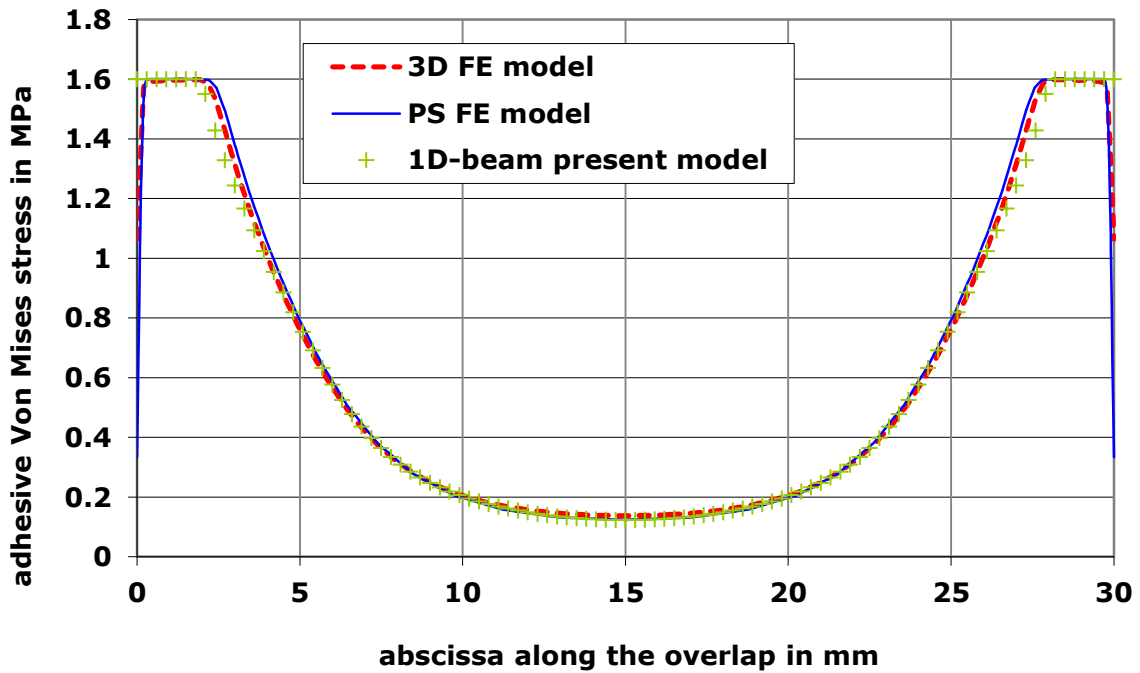


Figure 19. Comparison of the adhesive Von Mises stress distribution along the overlap between the 1D-beam present model and PS and 3D FE models, on a balanced structure.

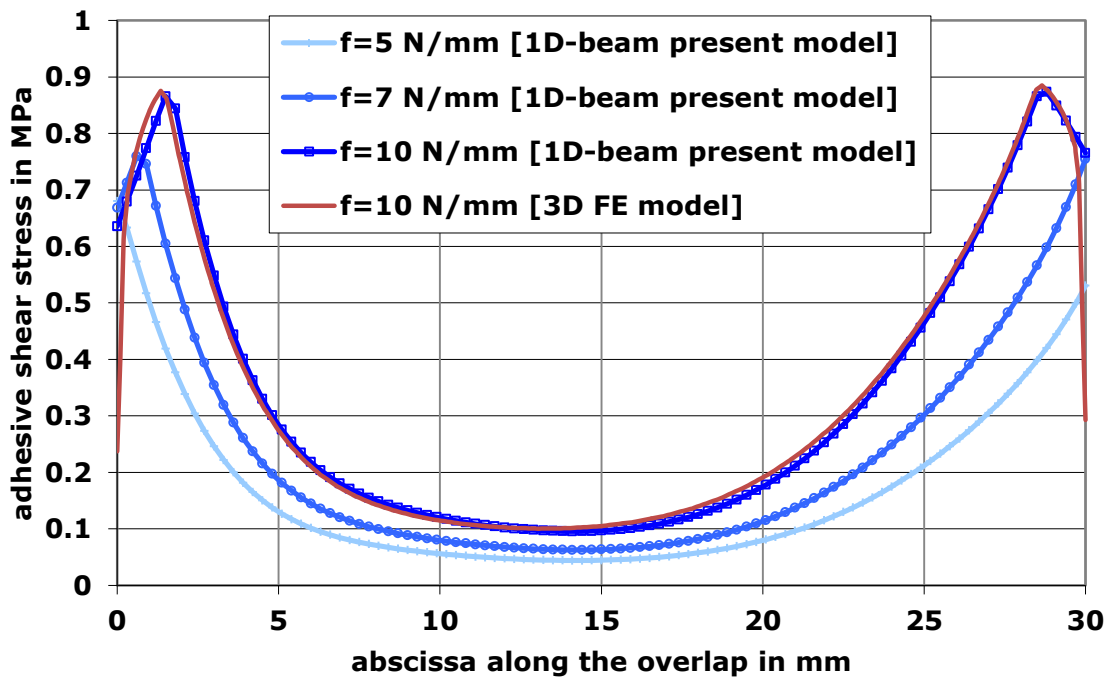


Figure 20. Comparison of the adhesive shear stress distribution along the overlap between the 1D-beam present model and PS and 3D FE models, on an unbalanced structure. The distributions at various intermediated applied forces are shown.

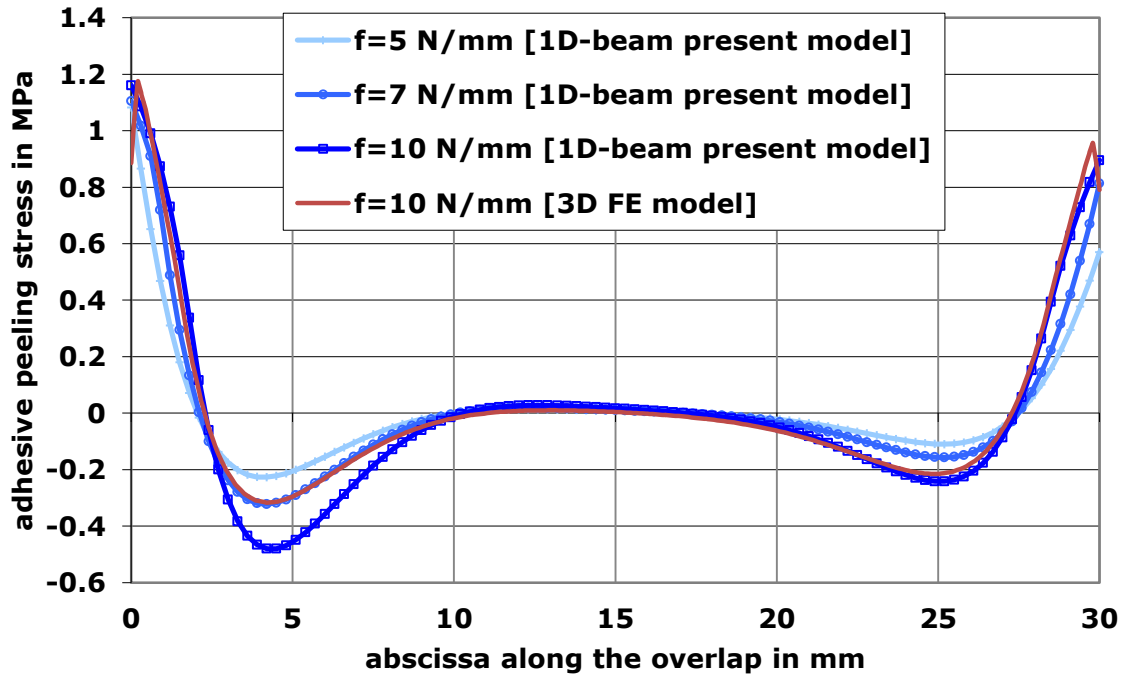


Figure 21. Comparison of the adhesive peeling stress distribution along the overlap between the 1D-beam present model and PS and 3D FE models, on an unbalanced structure. The distributions at various intermediated applied forces are shown.

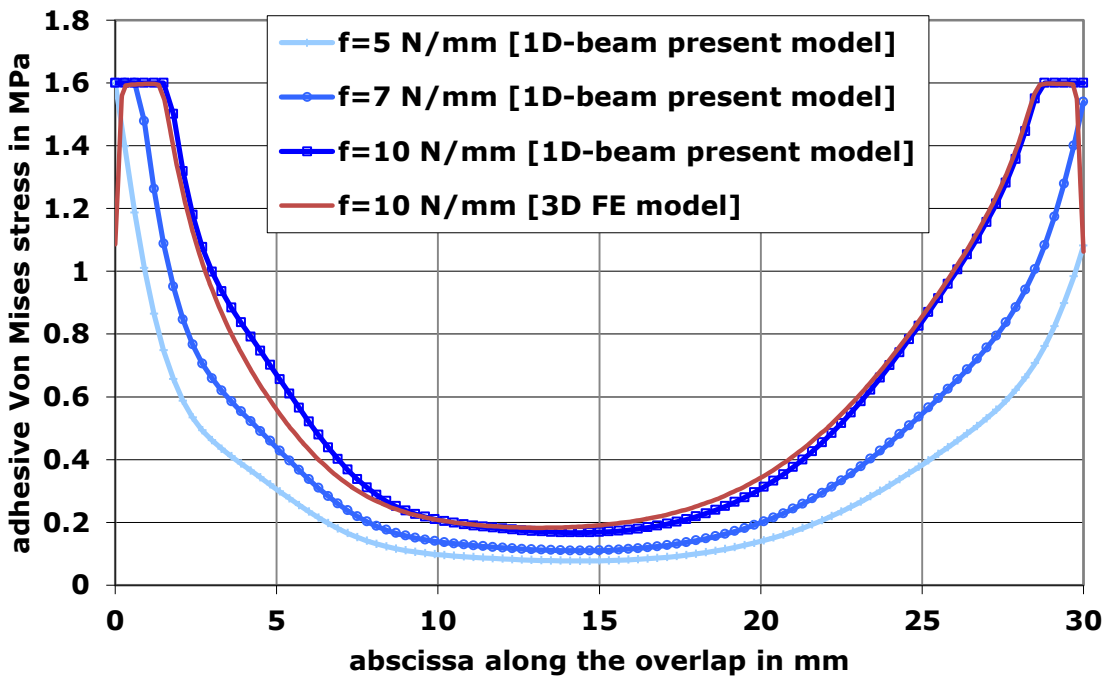


Figure 22. Comparison of the adhesive Von Mises stress distribution along the overlap between the 1D-beam present model and PS and 3D FE models, on an unbalanced structure. The distributions at various intermediated applied forces are shown.

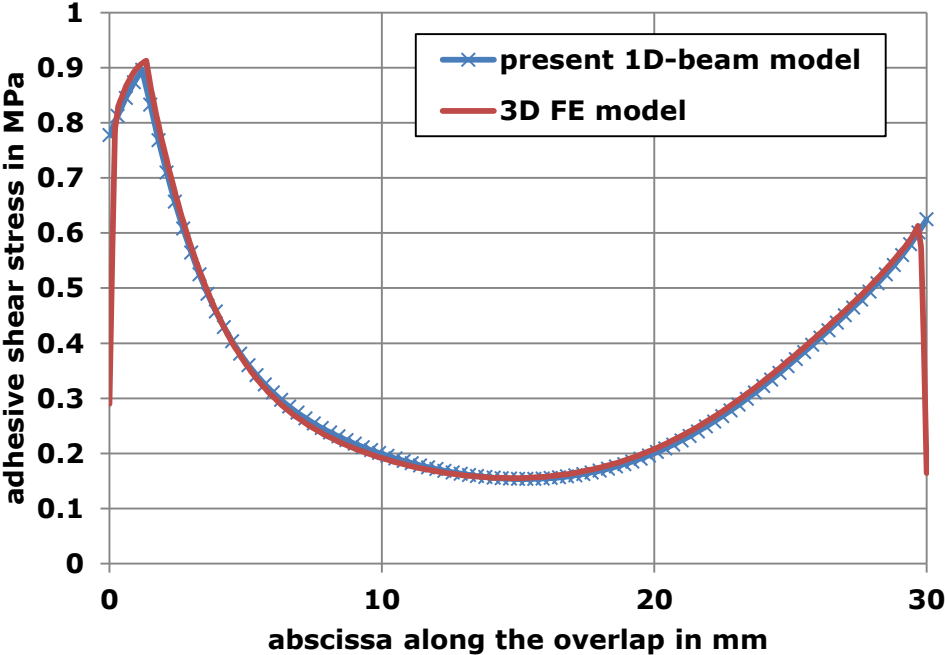


Figure 23. Comparison of the adhesive shear stress distribution along the overlap between the 1D-beam present model and 3D FE models, on an unbalanced structure.

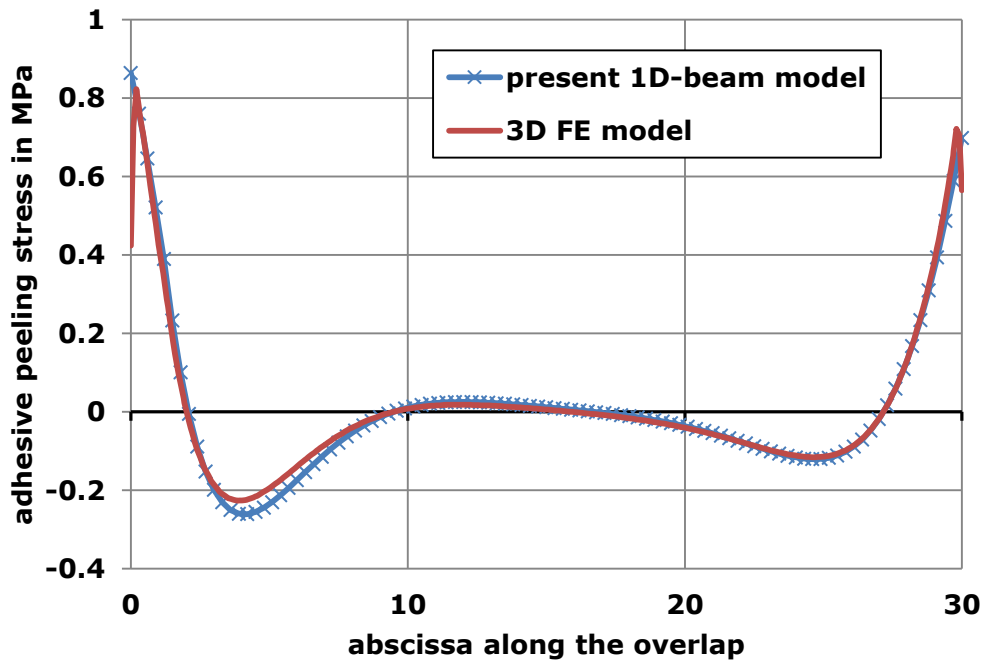


Figure 24. Comparison of the adhesive peeling stress distribution along the overlap between the 1D-beam present model and 3D FE models, on an unbalanced structure.

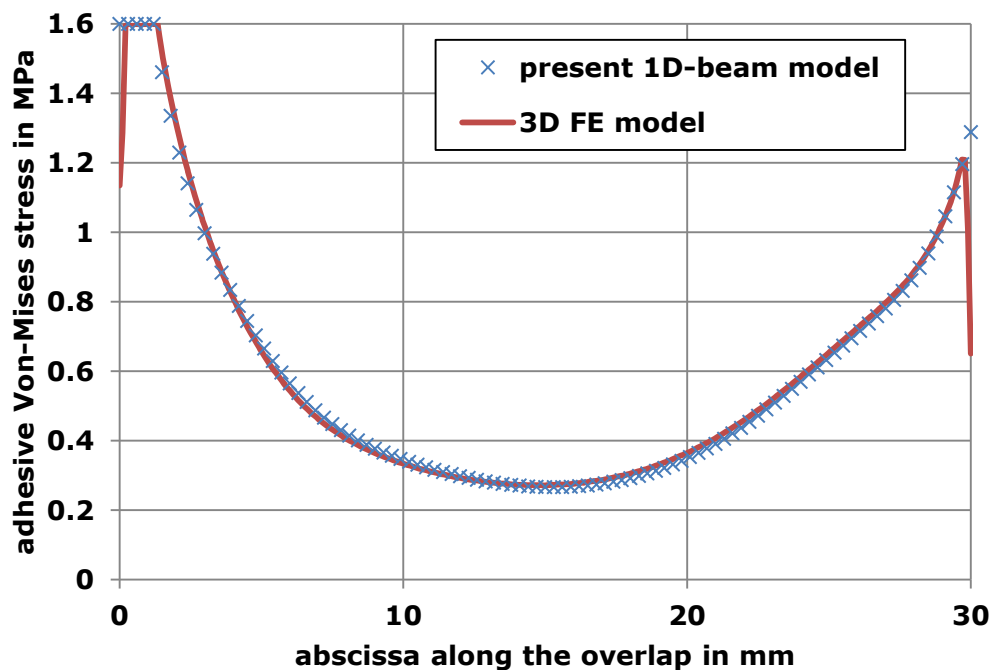


Figure 25. Comparison of the adhesive Von Mises stress distribution along the overlap between the 1D-beam present model and 3D FE models, on an unbalanced structure.

LIST OF TABLE CAPTIONS

Table 1. Geometrical and mechanical parameters of the nominal single-lap joint under consideration.

Table 2. Relative difference to the case with 32 elements, when the number of elements in the adhesive thickness varies.

Table 3. Relative difference to the FE predictions, when the adherend stiffness varies

Table 4. Relative difference to the FE predictions, when the adhesive stiffness varies.

Table 5. Comparisons of computation times between the 3D FE models and the 1D-beam model (1.3 s).

b	e	$e_1=e_2$	L	$l_1=l_2$	E	$E_1=E_2$	ν	$\nu_1=\nu_2$
(mm)	(mm)	(mm)	(mm)	(mm)	(MPa)	(MPa)		
1	0.4	2.4	30	151.5	2208	72000	0.38	0.33

Table 1. Geometrical and mechanical parameters of the nominal single-lap joint under consideration.

relative difference to the case with 32 elements		
number of elements	shear stress peak	peeling stress peak
2	-3.94%	25.8%
4	-1.16%	2.80%
8	-0.559%	-1.83%
16	-0.361%	0.372%

Table 2. Relative difference to the case with 32 elements, when the number of elements in the adhesive thickness varies.

relative difference to the 3D FE model predictions		
E1/E2	shear stress peak	peeling stress peak
0.5	0.642%	-4.93%
1	-2.57%	-1.46%
2	-3.53%	7.41%
3	-1.83%	5.00%

Table 3. Relative difference to the FE predictions, when the adherend stiffness varies.

relative difference to the 3D FE model predictions		
adhesive thickness	shear stress peak	peeling stress peak
0.1 mm	0.336%	-18.7%
0.2 mm	1.25%	-8.25%
0.3 mm	0.224%	1.56%
0.4 mm	-2.25%	3.16%
0.5 mm	-0.520%	4.61%

Table 4. Relative difference to the FE predictions, when the adhesive stiffness varies.

3D FE models	number of elements in the adhesive thickness				
	2	4	8	16	32
computation time in s	6.40E+01	4.30E+02	3.90E+03	7.42E+04	3.08E+05
number of times higher than for 1D-beam model	49	331	2996	57099	237231

Table 5. Comparisons of computation times between the 3D FE models and the 1D-beam model (1.3 s).